Lithos 282–283 (2017) 82–97

Contents lists available at ScienceDirect

Lithos

journal homepage: www.elsevier.com/locate/lithos

Magmatic garnet in the Cordilleran-type Galiléia granitoids of the Araçuaí belt (Brazil): Evidence for crystallization in the lower crust

F. Narduzzi [a,b,*], F. Farina [a,c], G. Stevens [b], C. Lana [a], H.A. Nalini Jr. [a]

[a] Applied Isotope Research Group, Departamento de Geologia, Escola de Minas, Universidade Federal de Ouro Preto, Campus Universitário Morro do Cruzeiro s/n, 35400-000 Ouro Preto, MG, Brazil
[b] Centre for Crustal Petrology, Department of Earth Science, University of Stellenbosch, Private Bag X1, 7602 Stellenbosch, South Africa
[c] University of Geneva, Department of Earth Sciences, Rue des Maraîchers 13, 1205 Geneva, Switzerland

ARTICLE INFO

Article history:
Received 9 September 2016
Accepted 25 February 2017
Available online 6 March 2017

Keywords:
Grossular-rich magmatic garnet
Magmatic epidote
High pressure crystallization
Cordilleran-type Galiléia granitoids
Araçuaí Orogen

ABSTRACT

Magmatic garnet, together with epidote, is a rare mineral association in cordilleran-I-type granitoids and of special petrogenetic significance. The metaluminous to slightly peraluminous (ASI = 0.97–1.07) Galiléia batholith (Brazil) is a large (ca. 30,000 km^2), Neoproterozoic (ca. 632–570 Ma) weakly foliated calc-alkaline granitoid body, characterized by the widespread occurrence of garnet (grossular 25–43 mol%) and epidote (pistacite 9.3–22.7 mol%). Field, petrographic and mineral chemical evidence indicates that garnet, epidote, biotite as well as white mica crystals (low-Si phengite), are magmatic. There is no difference in bulk rock major and trace element composition between the Galiléia granitoids and other garnet-free cordilleran-type granitoids worldwide. This evidence strongly suggests that the origin of the uncommon garnet + epidote parageneses is related to the conditions of magma crystallization, such as pressure, temperature and water content. Comparison between the mineral assemblages and mineral compositions from this study and those recorded in crystallization experiments on metaluminous calc-alkaline magmas, as well as within garnet-bearing metaluminous volcanic rocks and granitoids, indicates that the supersolidus coexistence of grossular-rich garnet, epidote and white mica is consistent with magma crystallization at pressures greater than 0.8 GPa (above 25 km depth) and at temperatures below 700 °C, i.e. near the water saturated solidus. Furthermore, resorption textures around garnet (plagioclase ± quartz coronas) and epidote suggest that these minerals have been partially consumed prior to complete crystallization. These findings demonstrate that at 630 Ma the crust underneath the Araçuaí Orogen was already at least 25–30 km thick and relatively cool. However, this contrasts with the marked high heat flow registered from the neighbour Carlos Chagas Batholith located 50 km to the east. In fact such granitoids record granulite-facies metamorphism at the same pressure and time (ca. 570 Ma) of Galiléia granitoids crystallization. Thus, a more suitable geodynamic scenario is required in order to explain these two contrasting thermal regimes within the same orogen. Eventually, field, petrographic and mineral chemical analogies with similar garnet-bearing granitoids located in the fore-arc settings of the British Columbia subduction zone, possibly imply that the Galiléia granitoids represent "rare" garnet- and epidote-bearing metaluminous Cordilleran-I-type granites which can only form in a fore-arc setting.

1. Introduction

Garnet is a common minor component of peraluminous granites formed via partial melting of Al-rich metasedimentary rocks (i.e. S-type granites). In these rocks, garnet has been shown to be commonly peritectic, produced by biotite incongruent melting of the metapelitic source of the S-type magma, or due to partial melting of metasedimentary country rock which the magma intruded (Erdmann et al., 2009; Lackey et al., 2012; Melo et al., 2017). Furthermore, garnet has also been proposed to represent entrained crystals from the source, that were not involved in the anatectic process (i.e. a resistate crystal, Vernon, 2007) or a xenocryst incorporated from the wall rock during the ascent and emplacement of the granitic body (Clarke, 2007). On the other hand, many studies have shown that garnet in S-type granites can also be magmatic in origin (e.g. Allan and Clarke, 1981; Barnes et al., 2012; Dalquist et al., 2007; Harrison, 1988; Lackey et al., 2012; Miller and Stoddard, 1981; Villaros et al., 2009). In addition, when subjected to metamorphism at suitable conditions, granites may develop metamorphic garnet. A good example is reported by Vielzeuf and Schmidt (2001), where Hercynian granitoids subjected to high pressure metamorphism during Alpine orogenesis developed garnet aureoles around biotite and plagioclase.

* Corresponding author at: Applied Isotope Research Group, Departamento de Geologia, Escola de Minas, Universidade Federal de Ouro Preto, Campus Universitário Morro do Cruzeiro s/n, 35400-000 Ouro Preto, MG, Brazil.
E-mail address: narduzzi13@gmail.com (F. Narduzzi).

http://dx.doi.org/10.1016/j.lithos.2017.02.017
0024-4937/

In metaluminous cordilleran-type granites as well as in metaluminous volcanic rocks, garnet is extremely rare and few natural occurrences have been reported in the literature (e.g. Bach et al., 2012; Barnes and Allen, 2006; Dawes and Evans, 1991; Day et al., 1992; Evans and Vance, 1987; Harangi et al., 2001; Samadi et al., 2014). Crystallization experiments (e.g. Alonso-Perez et al., 2009; Green, 1972, 1977, 1992; Green and Ringwood, 1968; Schmidt, 1993; Schmidt and Thompson, 1996) on metaluminous andesitic and tonalitic to granodioritic compositions show that garnet is stabilized at high pressures and at low temperatures, in magmas that are water-rich (typically in the range of 5–10 wt.% H_2O). The rare occurrence of garnet in such compositions in the plutonic record suggests that these conditions are rarely achieved (or preserved) in nature. Metaluminous granites and volcanic rocks with dacitic–rhyolitic composition can also be characterized by another uncommon magmatic mineral: epidote (Brandon et al., 1996; Schmidt, 1993; Schmidt and Poli, 2004; Schmidt and Thompson, 1996; Zen and Hammarstrom, 1984a, 1984b). More than a decade ago, Schmidt and Poli (2004) reported 19 occurrences worldwide. Since then an increasing number of scientific works reported its presence in other cordilleran-type granitic plutons and batholiths. As with garnet, epidote can be either metamorphic or magmatic. Magmatic epidote is commonly interpreted to indicate crystallization at moderate- to high-pressures (>0.6 GPa), with water saturation of the magma (≥10 wt.% of H_2O) (Schmidt and Thompson, 1996). Experimental evidence (Holdaway, 1972; Liou, 1973; Schmidt and Poli, 2004; Schmidt and Thompson, 1996) indicates that epidote stability is dependent on melt composition and fO_2 state, with crystallization being favoured in metaluminous granodioritic to tonalitic compositions in a relatively oxidized environment (i.e. NNO oxygen buffer). In addition, epidote appears to crystallize together with garnet only above approximately 1.2 GPa (Schmidt and Thompson, 1996). We combined information on occurrences of magmatic garnet (Samadi et al., 2014) and epidote (Schmidt and Poli, 2004) in metaluminous intrusives and volcanic rocks worldwide and there appear to be only few localities where magmatic garnet and epidote have crystallized together. These include: the garnet–epidote bearing dikes cropping out in the Front Range, Colorado (Dawes and Evans, 1991; Evans and Vance, 1987); the Dehnow pluton, north east Iran (Samadi et al., 2014); the Bushy Point Granites, south eastern Alaska (Arth et al., 1988; Zen and Hammarstrom, 1984a, 1984b); the Jinshan Intrusion associated with the Dabie Orogenic belt, China (e.g. Xu et al., 2013) and the subject of this study, the 30,000 km^2 Neoproterozoic Cordilleran-type Galiléia Batholith, located within the Araçuaí Orogen, Brazil (Mondou et al., 2012; Nalini, 1997; Nalini et al., 2000, 2005, 2008; Vauchez et al., 2007). Garnet and epidote-bearing assemblages have been reported throughout the Galiléia batholith but the origin of both minerals has not been accurately constrained. Detailed field and petrographic investigations coupled with mineral chemistry, whole rock geochemistry and comparison with the assemblages and mineral compositions produced in high pressure experiments, are used here to shed light on the origin of garnet and epidote in the Galiléia batholith.

2. Geological background

2.1. General background of the Araçuaí Orogenic Belt

The Araçuaí Orogenic Belt, together with its African counterpart (the West Congolian Belt), was formed during the Brasiliano/Pan-African orogeny (ca. 640–520 Ma; e.g. Alkmim et al., 2006). This orogen, located in south-eastern Brazil (Fig. 1a), lies between the Atlantic Ocean and the São Francisco Craton. Different tectono-stratigraphic schemes have been proposed to describe the architecture of this orogen. Pedrosa-Soares et al. (2001) and Pedrosa-Soares and Wiedemann-Leonardos (2000) proposed its subdivision into external, internal and northern domains, while Mondou et al. (2012) and Vauchez et al. (2007) adopted another subdivision (Fig. 1b) defining a Western Domain (or Western Mylonitic Unit), a Central Domain (or Central Plutonic Unit) and an Eastern Domain (or Anatectic Unit). Each domain is separated through major thrust zones (Fig. 1b; e.g. Vauchez et al., 2007). The Western Domain, which has been thrust over the eastern São Francisco Craton (mostly made up of gneiss and Al-quartzites), consists of high-temperature (~750 °C) and relatively low-pressure (~0.6 GPa) metasedimentary mylonites crosscut by abundant syn-kinematic garnet–cordierite-bearing leucocratic veins (570–580 Ma, LA-ICP-MS U–Pb zircon and monazite ages; Petitgirard et al., 2009). The Central Domain is mainly represented by Neoproterozoic (ca. 632–570 Ma) I-type granitoids which intrude the Paleoproterozoic basement (ca. 2.2–2.0 Ga) represented by the Pocrane gneiss Complex, and by the arc-related Rio Doce metasediments (Fig. 1c) (Gonçalves et al., 2014 and reference therein). According to Pedrosa-Soares et al. (2001) and Pedrosa-Soares et al. (2011) the granitoids and the metasediments are grouped together into the granitic 1 (G1) supersuite and are thought to be related to the pre-collisional stages of the Brasiliano orogeny that build up the Araçuaí orogen (Pedrosa-Soares et al., 2001). The Eastern Domain is subdivided into the Nova Venecia complex composed of migmatites, granulites and granites (e.g. Richter et al., 2015) and into the Carlos Chagas batholith characterized by peraluminous S-type granitoids (e.g. Melo et al., 2017). These rocks, according mainly to their location, ages and geochemistry (Pedrosa-Soares et al., 2001), are subdivided in syn-collisional (G2, 585–560 Ma), late collisional (G3; 560–530 Ma) and post-collisional (G4–G5, 530–480 Ma) supersuites. Small igneous bodies belonging to the G2, G4 and G5 supersuites, intrude into the Central Domain.

2.2. The Galiléia Batholith

The granitoids of the G1 supersuite (Fig. 1b, c) consist of orthopyroxene-rich (i.e. charnockites) and orthopyroxene-free granites and granodiorites, the latter forming the so-called Galiléia Batholith and displaying variable amounts of mafic microgranular enclaves (MME) (e.g. Gonçalves et al., 2014). The batholith extends roughly north–south for ca. 600 km, almost the entire length of the Araçuaí orogen, covering an area of approximately 30,000 km^2 (Fig. 1a) (Gonçalves et al., 2014; Pedrosa-Soaeres et al., 2011; Pedrosa-Soares et al., 2001; Vauchez et al., 2007). Based on field evidence, mineral textural studies and geochemical features, Gonçalves et al. (2014) have recently further subdivided the Galiléia batholith into a suite of enclave-rich tonalite–granodiorite rocks and a suite of enclave-poor tonalitic to granitic rocks. These two suites, appear to occur throughout the whole batholith (Fig. 1b and c). Geochemically, the opx-free granitoids resemble medium- to high-K metaluminous Cordilleran-type granitoids, and are interpreted as being produced during the Rio Doce arc-related magmatism; they are suggested to be derived from the partial melting of the Paleoproterozoic basement due to underplating of mantle derived magmas (e.g. Gonçalves et al., 2014). However, assimilation of host rocks, fractional crystallization during the ascent of mantle-derived magmas, or mixing between mantle derived magma with felsic magmas of crustal origin have also been proposed as possible processes that might have shaped the Galiléia igneous rocks (e.g. Gonçalves et al., 2014).

Recently, Tedeschi et al. (2016) presented new ages for the whole G1 granitoid suite and reviewed the age information available from previous studies. The entire age spectrum demonstrates that the G1 granitoids have magmatic zircon crystals indicating intrusion between 632 and 570 Ma. Tedeschi et al. (2016) identify three main intervals of crystallization ages: 632–605 Ma, 600–590 Ma and 585–570 Ma (Fig. 13 in Tedeschi et al., 2016), which have been suggested to represent three main periods of granitogenesis thus corresponding to three main phases of construction of the Rio Doce arc.

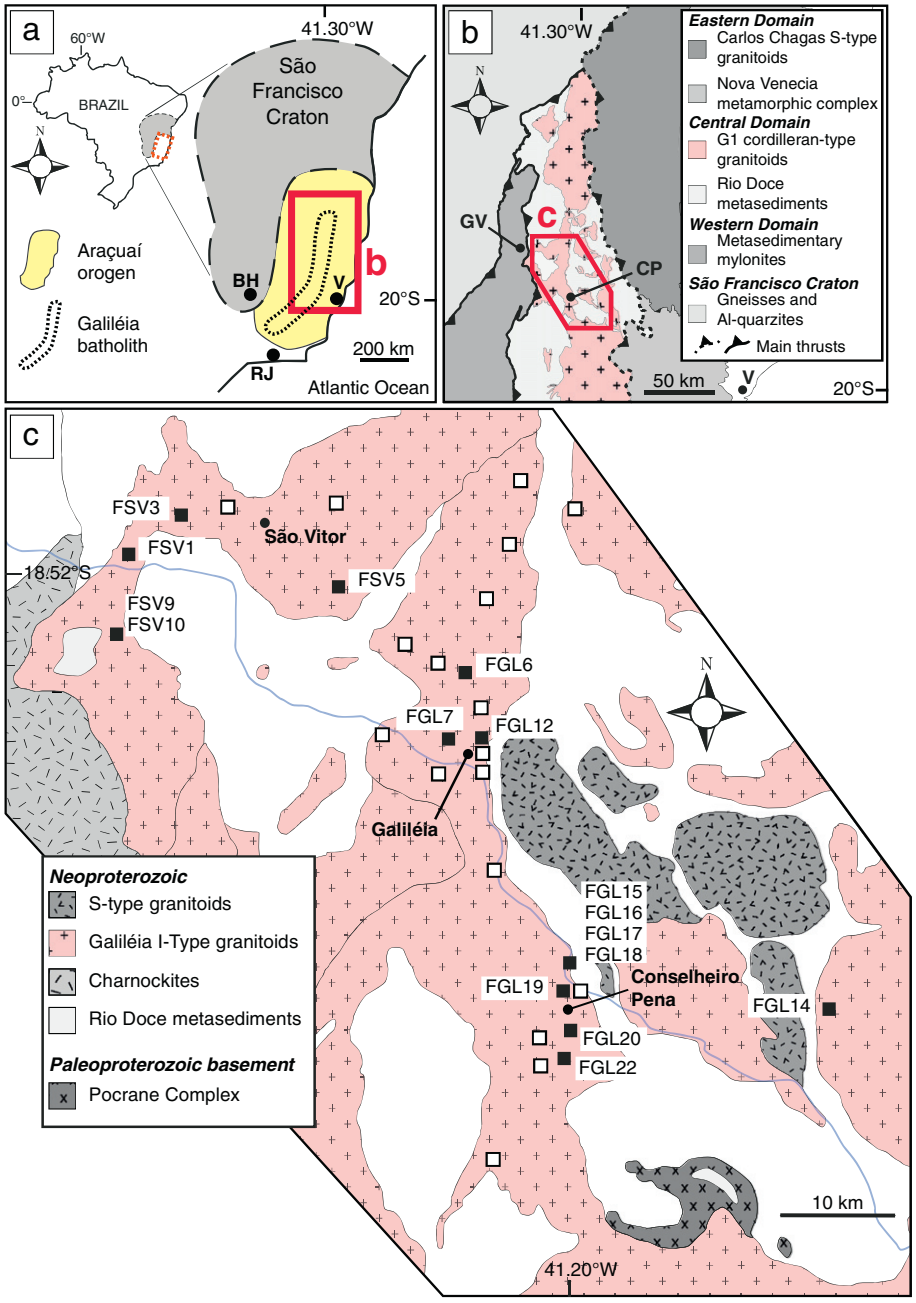

Fig. 1. Schematic geological map of the Araçuaí Orogen and Galiléia granitoids (modified after Vauchez et al., 2007). (a) Location of the Araçuaí Orogen (red rectangles) and Galiléia batholith in Brazil; SFC: São Francisco Craton; (b) Subdivision of the Araçuaí Orogen in Western, Central and Eastern domain while black bold and dotted lines are major thrusts separating each domain (after Vauchez et al., 2007); red polygon indicate the study area; (c) Geological map of the central part of the Galiléia batholith; In (a) and (b): BH: Belo Horizonte; CP: Conselheiro Pena; GV: Governador Valadares; RJ: Rio de Janeiro; V: Vitoria.

2.3. The Rio Doce metasedimentary host rocks

The Rio Doce metasediments are poorly studied. In the studied area an unpublished work (Vieira, 2007) has proposed that these rocks underwent medium pressure amphibolite facies metamorphism with pressure estimates from empirical geobarometry on garnet-bearing rocks of approximately 0.5 GPa. The study was conducted on areas far from the contact with the Galiléia granitoids. Cunningham et al. (1996) and Nalini et al. (2008) report that the Galiléia granitoids have both intrusive and tectonic contacts with the Rio Doce metasediments. Mondou et al. (2012) suggested also that intrusion was contemporaneous with pervasive deformation in the Rio Doce metasediments.

3. Results

This study focuses on the granites belonging to the enclave-rich unit in the central part of the Galiléia batholith (Fig. 1b and c), previously investigated by Gonçalves et al. (2014), Mondou et al. (2012), Nalini (1997), Nalini et al. (2000, 2005, 2008) and Vauchez et al. (2007). The study area covers ca. 4000 km^2. In this paper we use the name Galiléia granitoids to refer to the enclave-rich granitoids of the Galiléia batholith. A description of the analytical methods used as well as the complete dataset comprehensive of both mineral chemistry data and whole rock compositions are presented in the Online Supplementary Material.

3.1. Field relationships

The studied rocks consist of medium-grained tonalites, granodiorites, and subordinate granites (Fig. 2), that are either equigranular or porphyritic, with the latter texture reflecting the presence of feldspar crystals (≥1 cm) larger than the respective matrix minerals. Less commonly, coarse- and fine-grained examples of tonalite and granodiorite also occur. The granitoids are typically weakly deformed showing a foliation that is defined by the orientation of biotite and amphibole crystals and marked by the long axis of stretched mafic enclaves (Fig. 2a and b). The foliation has a dip ranging from 50° to 80° towards NE or SW (see also Nalini et al., 2008). Some outcrops display evidence for the coexistence of slightly different varieties of granite, one more melanocratic and the other more leucocratic (Fig. 2c). Based on petrographic and field observations, major rock-forming minerals are plagioclase (32–42 vol.%), quartz (15–33 vol.%) and K-feldspar (1.5–14 vol.%). Biotite, amphibole and garnet are the main mafic minerals (see also Gonçalves et al., 2014), with biotite being the most abundant, forming up to 19 vol.%. Hornblende is not ubiquitous and occurs in ca. 80% of the outcrops, sometimes forming crystals of up to 1 cm in size and making up 3–18 vol.% of the rock. Garnet forms a minor component of the rocks up to 2 vol.%. A detailed description of the procedure used for the vol.% estimation is given in Section 3.1.1. Accessory minerals are epidote, allanite, titanite, apatite, zircon, pyrite and pyrrhotite, while oxide minerals such as magnetite and ilmenite are rare.

Tonalites and granodiorites are characterized by different amounts of mafic microgranular enclaves (MME) (Fig. 2a, b, and d). MMEs can be lobate, stretched, lenticular, and sometimes showing bridge structures (Fig. 2a, b, e and f, respectively). In agreement with Nalini et al. (2008) the enclaves are generally stretched along a N30–60°W

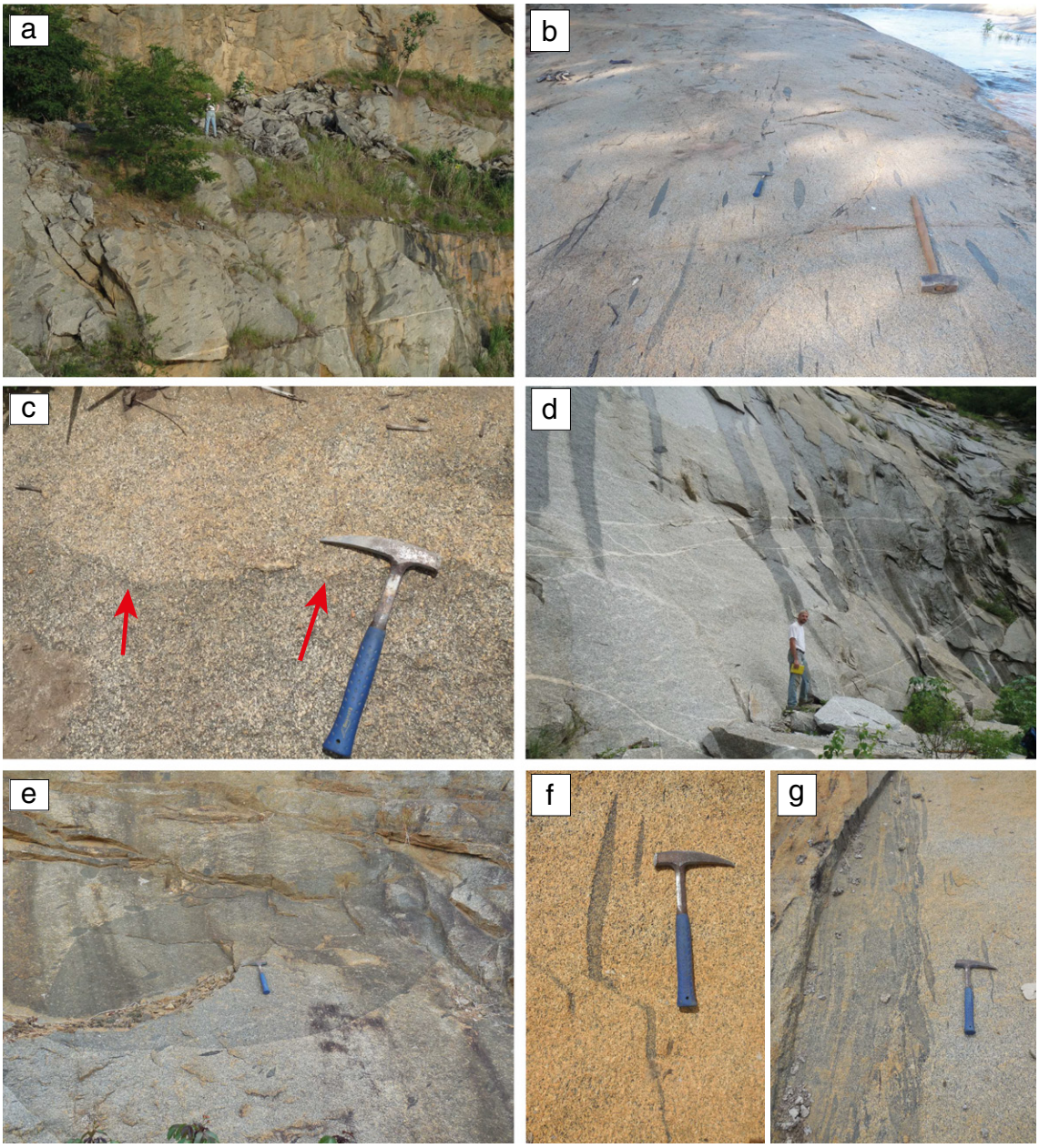

Fig. 2. Field features of the Galiléia granitoids. Typical appearance of a: (a) garnet-bearing enclave-rich granitoids, (b) garnet-free granitoid containing widespread MMEs (≥7 MME/m^2), (c) coexistence of a melanocratic and leucocratic granitic magmas as indicated by the red arrows, (d) MME-free garnet-bearing granite; (e) rounded composite enclave reaching almost 4 m in width; (f) stretched enclaves. Note the bridge structure, possibly due to deformation in sub-magmatic state; (g) stretched enclaves swarm in a composite dyke. Brown and blue hammer are 60 and 32 cm in length, respectively.

direction and exhibit variable aspect ratios (length/width = 2:1 to ca. 10:1). The most stretched enclaves occur in outcrops where the granitoids are both strongly and weakly deformed (Fig. 2a and b, respectively). The stretched mafic enclaves in the weakly deformed granites (i.e. Fig. 2b) have aspect ratios that are inconsistent with the weak fabrics in the matrix around the enclaves, confirming that they represent a strong magmatic state lineation produced by magma flow (e.g. Paterson et al., 1998). In the least deformed outcrops, MMEs have also variable sizes reaching occasionally up to 4 m in length (Fig. 2e), while in other areas they are small (<2 cm) and can easily be misinterpreted as biotite clots. In order to quantify their abundance, MME counting (MME/m^2, Fig. 3a) was performed using an area of 5 × 5 m, for a total of 30 outcrops. Where possible, more than one area was analysed for each outcrop. In the counting procedure, only those MMEs that were at least for three-quarters of their area inside the grid were counted. MME counts range between 0 and 7 MME/m^2, with values between 1.70 and 3.30 MME/m^2 being typical (Fig. 2a, c, d).

3.1.1. Garnet abundance and distribution

Garnet is widespread in the Galiléia Batholith and garnet counting (garnet crystals/m^2, Fig. 3b) was performed in order to describe the variation in the number of macroscopically visible crystals per m^2; a grid area of 10 × 20 cm was used. Counting was conducted for 30 outcrops. In this case, up to five areas were counted per each outcrop, with the grids randomly distributed on the surface of the outcrop and separated by distances of more than 1 m in order to avoid counting bias. Within individual outcrop the garnet crystal/m^2 counts do not vary significantly. Consequently, the average values calculated are assumed to be representative for each outcrop.

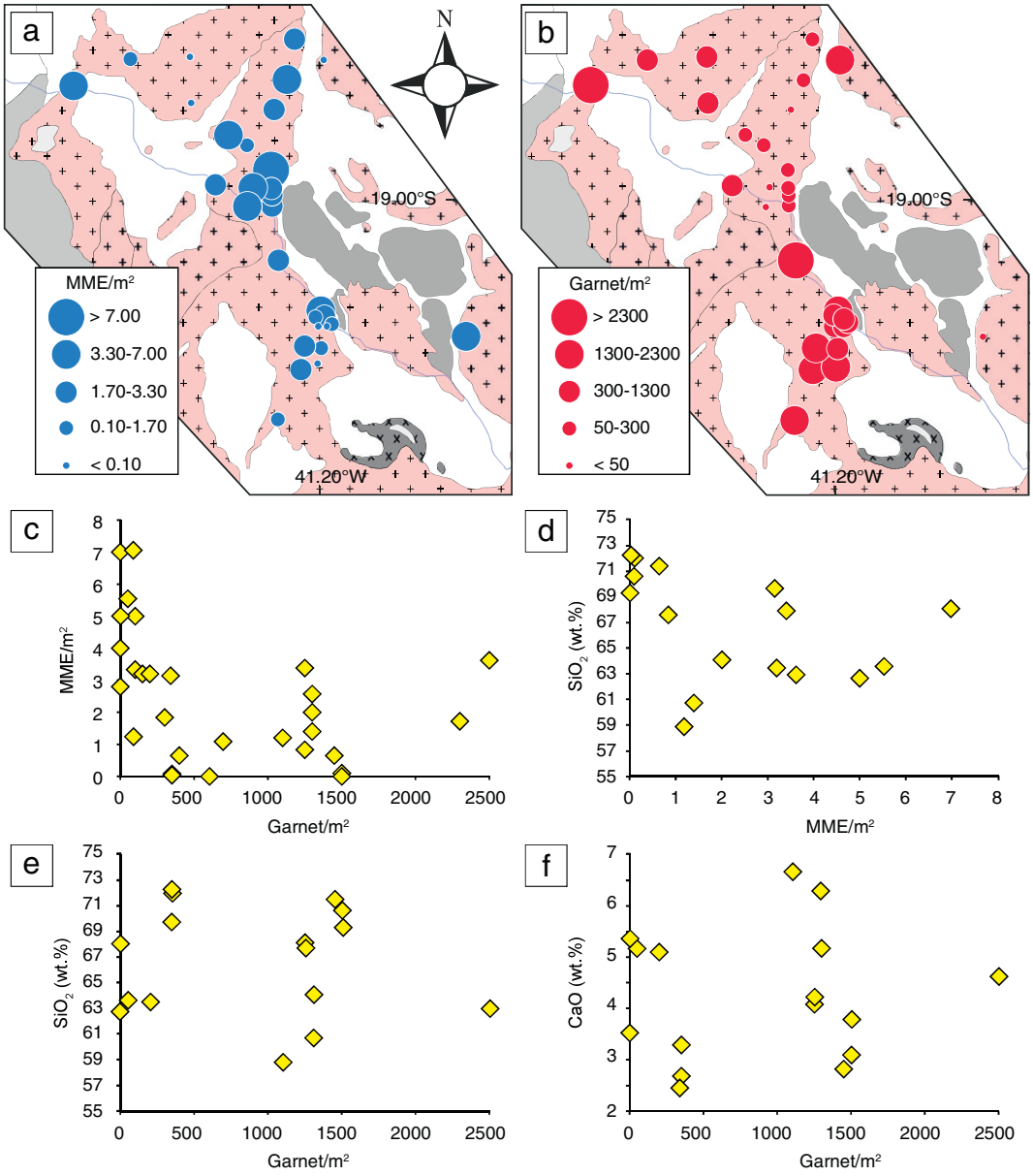

Fig. 3. Garnet and mafic enclave counting. MME (a) and garnet (b); counts for 30 outcrops. The grids used for counting were 25 m^2 (5 × 5 m) for MMEs and 200 cm^2 (10 × 20 cm) for garnets (later converted in m^2). The lowest garnet counts (Grt/m^2 < 50) represent 0 vol.%, while the highest reach almost 2 vol.% of the outcrop. Note that the area is the same as in Fig. 1c and this counting procedure covered all the entire area, that is ca. 4000 km^2; (c) Average garnet vs. MME counts; (d) and (e) MME/m^2 and Grt/m^2 are plotted against granitoid SiO_2 content; in (f) the Grt/m^2 is plotted against the CaO (see the text for more explanation). Note that for some of the samples here plotted, the chemical analyses will be reported elsewhere.

The number of garnet crystals per m^2 varies from 0 to a maximum of 2500. This equates to a variation from 0 up to ca. 2 vol.%. Nevertheless, most of the batholith has a garnet crystal abundance between 300 and 1300 crystals/m^2. There is no relationship between garnet abundance and degree of rock deformation. Moreover, there is no relationship between the abundance of garnet crystals and proximity to contacts with the country rocks (Fig. 3b), nor with the presence of country rock xenoliths. Additionally, there is also no relationship between the number of garnet crystals and the abundance of mafic enclaves (Fig. 3c) or with the geochemistry of the rocks. In fact the MME and garnet abundance results in a scattered behaviour when compared with bulk rock SiO_2 and CaO concentrations (Fig. 3d, e and f). Garnet is found mostly in granodiorites with the exception of the only tonalite sampled. Garnet ranges in size from 1 to 6 mm with an average of less than 2 mm (Figs. 4 and 5). Crystals typically have a dark red core surrounded by an orange rim. In the field, garnet exhibits a range of habits that occur with different associations, irrespective of the degree of matrix deformation. These are: 1) anhedral to subhedral crystals mantled by or included in subhedral feldspars in porphyritic weakly deformed to non-deformed granitoids (Fig. 4a and b, respectively); 2) skeletal crystals showing evidence of resorption associated with plagioclase and biotite in textures that suggest that these minerals have replaced garnet (Fig. 4c) and 3) euhedral garnets in amphibole-bearing granitoids (Fig. 4d). Moreover garnet appears to also have been transferred from the granite to the MMEs during mingling between the felsic and intermediate to mafic magmas. This occurred directly as dispersed single crystals as well as after being included in subhedral feldspar (Fig. 4e).

3.2. Petrography

The Galiléia granitoids display four different ferromagnesian mineral associations which are reported in order of abundance: 1) biotite + garnet (Bt + Grt), 2) biotite + amphibole + garnet (Bt + Amp + Grt), 3) biotite + amphibole (Bt + Amp), and 4) biotite (Bt), with epidote ubiquitous in all these rocks.

3.2.1. Major and minor rock-forming phases

Biotite (Figs. 5 and 6) varies in colour from dark brown to reddish, with euhedral and subeuhedral habitus, rarely exceeding 2 mm; apatite, zircon and epidote are common inclusions. Biotite is also found as inclusions within garnet, amphibole and plagioclase. The colour of biotite inclusions is identical to the matrix biotite and these crystals are always smaller than 1 mm. In the MMEs, biotite always appears to be in textural equilibrium with the other minerals, and as in the granites, biotite defines the foliation.

The rocks contain several different types of plagioclase. The most common type is represented by subhedral crystals that vary in size from less than 1 mm up to 5 mm (Figs. 4, 5 and 6). These crystals are slightly zoned and show undulose extinction. Plagioclase (± quartz) coronas around garnet, as well as plagioclase inclusions within garnet, share these characteristics. Plagioclase also occurs as larger (10 to 15 mm) crystals that have euhedral to subhedral An-rich cores surrounded by more sodic rims (Fig. 6j); these crystals are also found within the MMEs (Fig. 6k). Cracked and zoned epidote can be found as inclusions within the plagioclase (Fig. 6c). The presence of plagioclase showing intragranular fractures filled by late magmatic minerals such as quartz and K-feldspar is also recognized. This possibly represents microfractures developed in the presence of late stage melt (Fig. 6l). Alkali-feldspars occur either as larger (0.5 to 5 mm) perthitic microcline or smaller interstitial (0.2–0.7 mm) crystals, showing undulate extinction and weak deformation, respectively. They are also included in garnets.

Amphibole is present in the granitoids as well as within MMEs, and always occurs with lower modal abundance than biotite. Amphiboles are euhedral to subhedral with sizes comprising between ca. 0.1 and 0.8 mm, although larger amphibole (>1 cm) also occurs. Inclusions in amphibole comprise biotite, plagioclase, apatite, zircon, titanite, ilmenite, primary sulphides, quartz and occasional epidote. Amphibole in the mafic enclaves displays a slightly more resorbed aspect relative to that in the granite, resulting in subhedral to anhedral habitus. Their colour and size are however comparable to those of the granitoids.

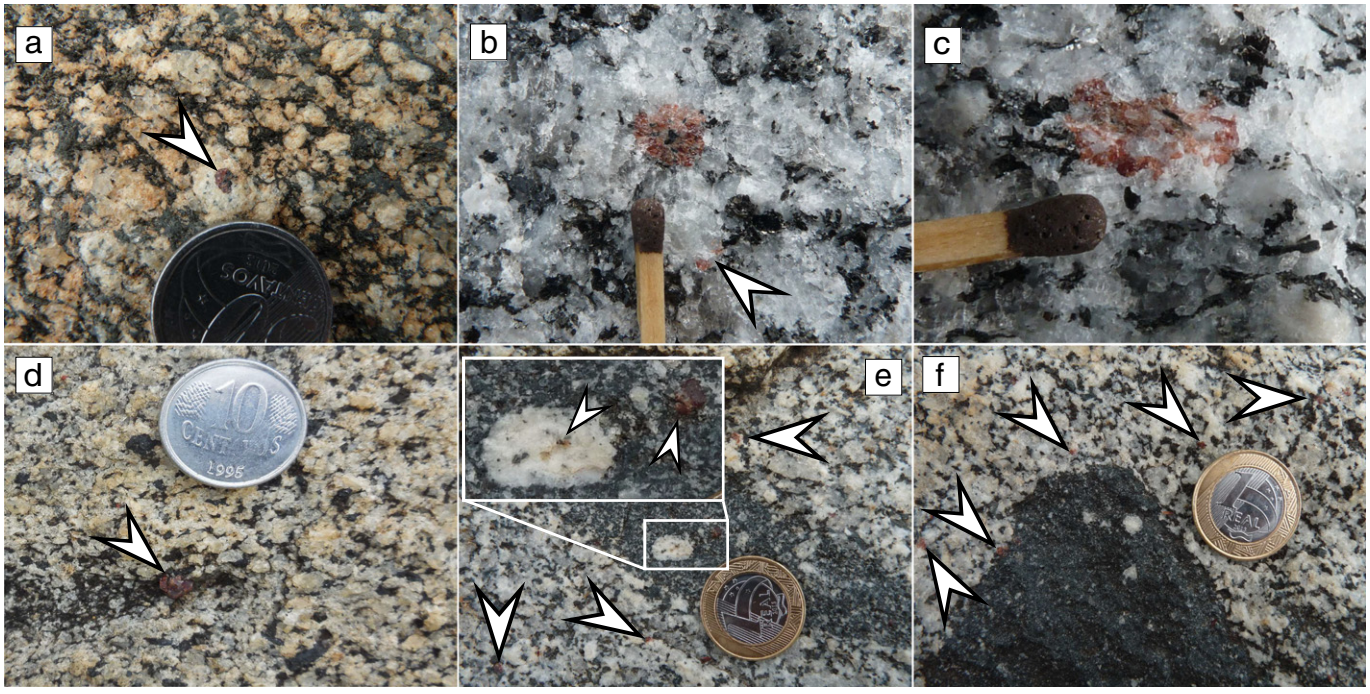

Fig. 4. Garnet field relationships. Garnets are indicated with arrows. Sizes are between 1 and 6 mm with an average of 3 mm; (a) anhedral garnet included in subhedral feldspar in weakly deformed granites; (b) subhedral radial garnet included in feldspar with evident biotite inclusion; (c) garnet in net disequilibrium and texturally associated with plagioclase feldspar and biotite; (d) euhedral garnet in amphibole bearing weakly deformed granite; (e) MME containing garnets occurring both as single crystals and included in subhedral feldspar; note the stretched character of the enclave hosted in weakly deformed granite; (f) garnet-free MME in garnet-bearing granites. The match head is 5 mm while grey and yellow coins are 2 and 2.5 cm, respectively.

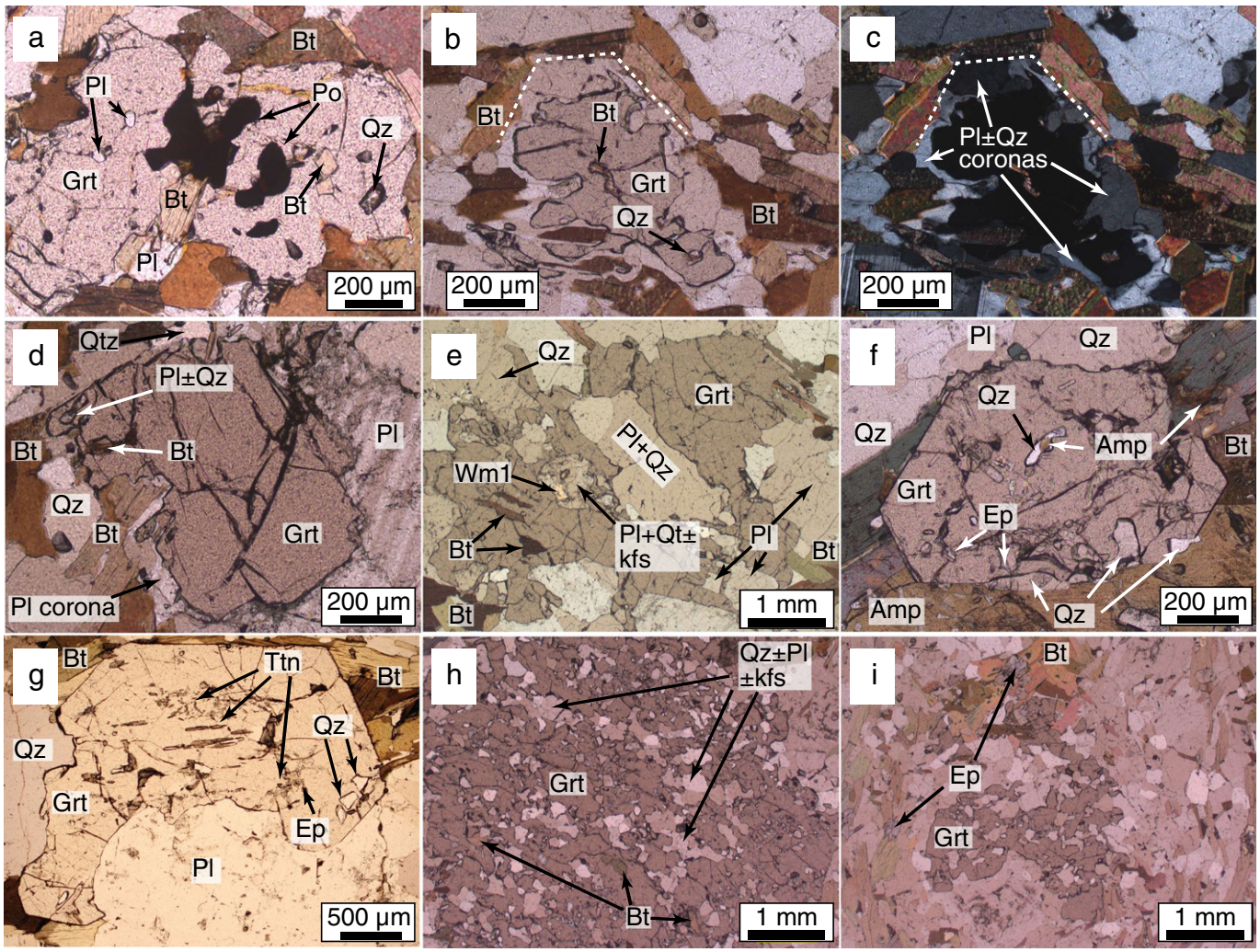

Fig. 5. Garnet petrography: (a) to (e) garnet in Bt + Grt granitoids; (f) and (g) garnets in Bt + Amp + Grt granitoids; (h) and (i) garnets in MMEs; (a) to (d) anhedral to subhedral garnets within the same thin section belonging to a slightly deformed granitoids; (a) inclusion-rich anhedral garnet having resorbed rims, mostly surrounded by biotites; note the random distribution of the inclusions; (b) and (c) inclusion-poor anhedral garnet with well-developed plagioclase ± quartz and biotite coronas pseudomorphosing previous garnet shape; (c) is at crossed nicols; (d) inclusion-poor subhedral garnets showing different levels of rims resorption and plagioclase coronas; inclusions are localized only at the top left coupled with the increasing in grossular content (cf. Fig. 7b); (e) anhedral–skeletal garnet within weakly deformed granites (cf. Fig. 4c) with inclusion of primary white mica (Wm1) replacing magmatic plagioclase (cf. Fig. 6f); (f) randomly-distributed inclusion-rich euhedral garnet showing weakly resorption as also highlighted in Fig. 7a; (g) inclusion-rich subhedral garnet in weakly deformed granitoids with evident plagioclase resorption; (h) garnet having spongy-like texture probably as a consequence of geochemical disequilibrium with respect the host MME; this texture is not evident for the garnets hosted in the granitoids; the mineral inclusions assemblage in this garnet (cf. Fig. 7c) as well as those from (a) to (g) matches the mineral matrix assemblage of the host granitoids; (i) garnet crystal in MMEs almost completely resorbed; eventually, despite belonging to weakly deformed granitoids, none of the garnets crystal show any pressure shadows or recrystallization front around their resorbed rims; Other explanations in the text. Mineral abbreviations as in Whitney and Evans (2010).

Garnet crystals are commonly cracked and as already evidenced from field observations, they exhibit different textures. Following their shapes, garnet crystals have been subdivided in two types: anhedral/skeletal and subhedral/euhedral. Except for a single rock (Fig. 5a–d), all the samples contain only one garnet type. It is noteworthy that no correlation between crystal shape and mineral assemblage of the granitoid has been observed (i.e. amphibole-bearing or amphibole-free granitoids) (cf. Fig. 5a–g). Additionally, and regardless of their shape, garnet crystals may or not contain inclusions. A subset of subhedral crystal garnets exhibit weakly to pronounced resorbed rims without any recrystallization or surrounding pressure shadow texture (Fig. 5a–g). Garnet is commonly mantled by plagioclase ± quartz coronas, which occasionally are surrounded by an external biotite corona, which in some cases pseudomorphs the original crystal, suggesting complex garnet replacement reactions (Fig. 5b, c). Inclusion assemblages within garnets comprise mostly quartz (30–36%), plagioclase (19–20%), titanite (15–16%), epidote (10–12%) and biotite (9–11%). White mica, apatite, zircon, and in rare cases amphibole, K-feldspar, primary sulphides and zoisite are also recognized (10–12%). The inclusions are randomly distributed within the garnet crystals and, with the exception of zoisite (Fig. 6f), the inclusion assemblage corresponds to the mineral association constituting the matrix of the granitoids (Figs. 5 and 7a, b). Garnet within the mafic enclaves displays spongy-like textures resulting from intense resorption of both rims and cores (Fig. 5h), thus suggesting that garnet crystals originally formed in the granite were transferred into the enclave. In this latter, in a more mafic and probably hotter magma, garnet was in strong disequilibrium (Fig. 5i). The few well-preserved garnet crystals within the MMEs host abundant inclusions of biotite, plagioclase, titanite, epidote and quartz (Figs. 5h, i and 7c), with these inclusions matching the mineralogical assemblage of the hosting granitoid rather than that of the MME. In particular, the amphibole crystals that form a significant fraction of the MMEs are never observed as inclusions in the garnets.

3.2.2. Main accessory phases

Epidote crystals are small (≤1 mm), with euhedral to subhedral shapes (Fig. 6a, b and c). In the granitoids and in the MMEs epidote appears in the matrix and as inclusions in biotite, plagioclase, garnet and

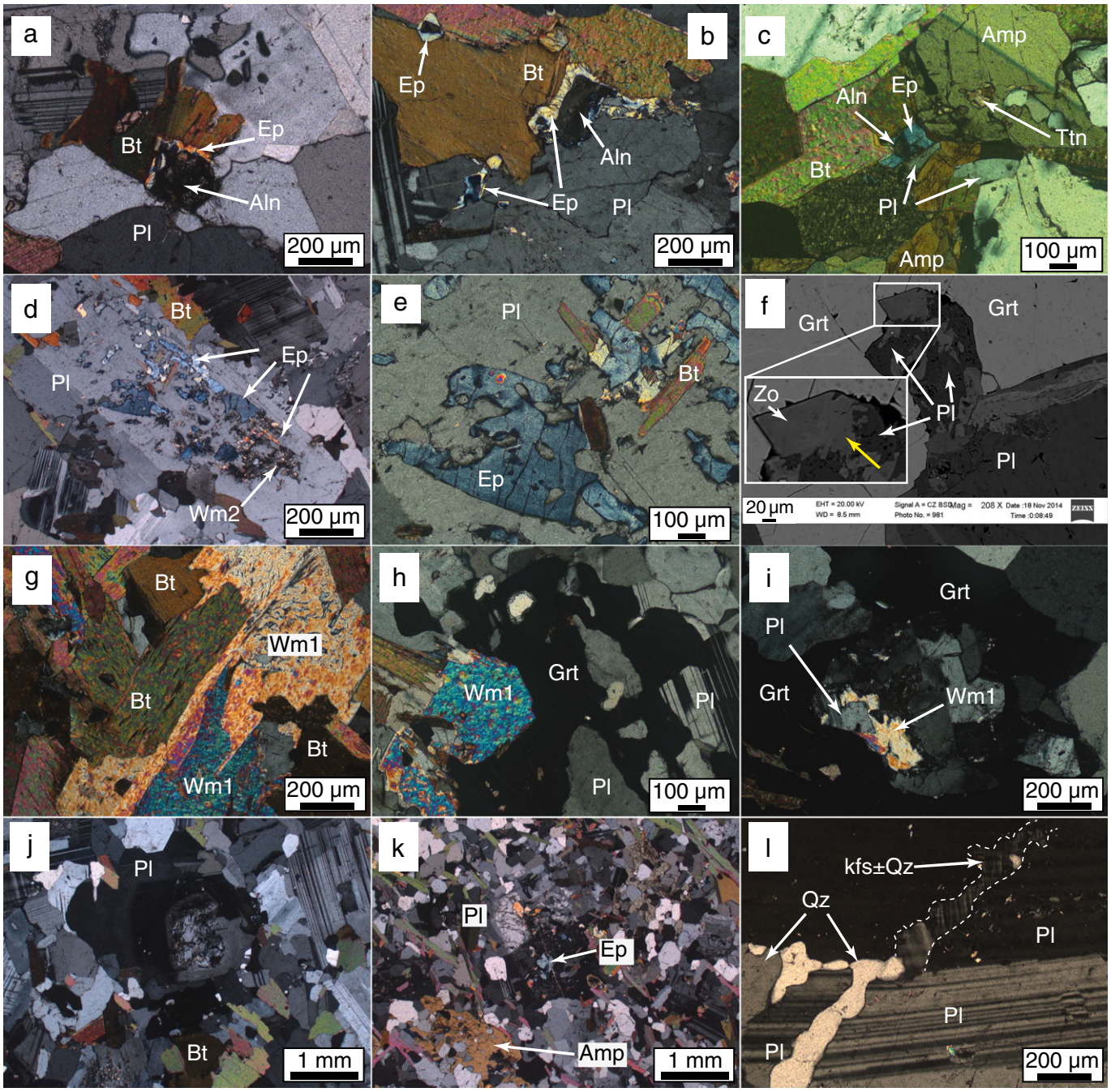

Fig. 6. General petrography. (a) and (b) Epidote in matrix crystallized between biotite and plagioclase while in (c) also between amphibole; note in (b) top left the well preserved epidote inclusion in biotite with evident allanite core; in the matrix epidote rim surrounding allanitic cores are preserved because mantled by biotite and absent due to plagioclase resorption; (d) and (e) epidote inclusions in plagioclase; these inclusions are skeletal/ragged, cracked, zoned and mostly have corroded rims; secondary white micas (Wm2) are sericitic micas; (f) zoisite inclusion in garnet, the latter being replaced by a plagioclase corona; zoisite in contact with garnet has a darker colour than the part of the crystal in contact with plagioclase; (g) primary white mica (Wm1) in matrix is replacing magmatic biotite; in (h) Wm1 is armoured by garnet; (i) Wm1 included in garnet while is replacing plagioclase; (j) and (k) plagioclase with An-rich cores surrounded by more sodic rims in granitoids and MME, respectively; (l) micro-fractured plagioclase filled by late stage quartz and K-feldspar. Except (f), all the other figures are in crossed nicols.

only rarely in amphibole. In the matrix, epidote rims surrounding allanite cores are generally zoned, and are located between amphibole, plagioclase and biotite and/or plagioclase and biotite (Fig. 6a, b and c, respectively). Epidote, like garnet, shows resorption textures, especially when in contact with plagioclase (Fig. 6a, b). Epidote inclusions (≤0.1 mm) (Fig. 6b top left) occasionally display allanite cores, and when hosted in biotite or hornblende, they usually show subhedral habitus. In plagioclase, epidotes are ragged with corroded, curvilinear sharp rims and cracks, which are not observed in the surrounding plagioclase (Fig. 6d and e). The latter features have been previously reported by Chang and Andronicos (2009) and Zen and Hammarstrom (1984a, 1984b) whose proposed contrasting interpretation. The epidote crystals are only rarely in between biotite and quartz in the Bt-free garnet granodiorite.

White mica is widespread within Bt + Grt bearing rocks. It is observed with a subhedral magmatic habitus forming crystals of up to ca. 1 mm in size (Fig. 6g) and as inclusions in garnet (Fig. 6f). Relatively large crystals of white mica are commonly associated with biotite (Fig. 6g) while small crystals (<0.3 mm) are often included in garnet or being armoured by it. This is evident by the sharp contact between

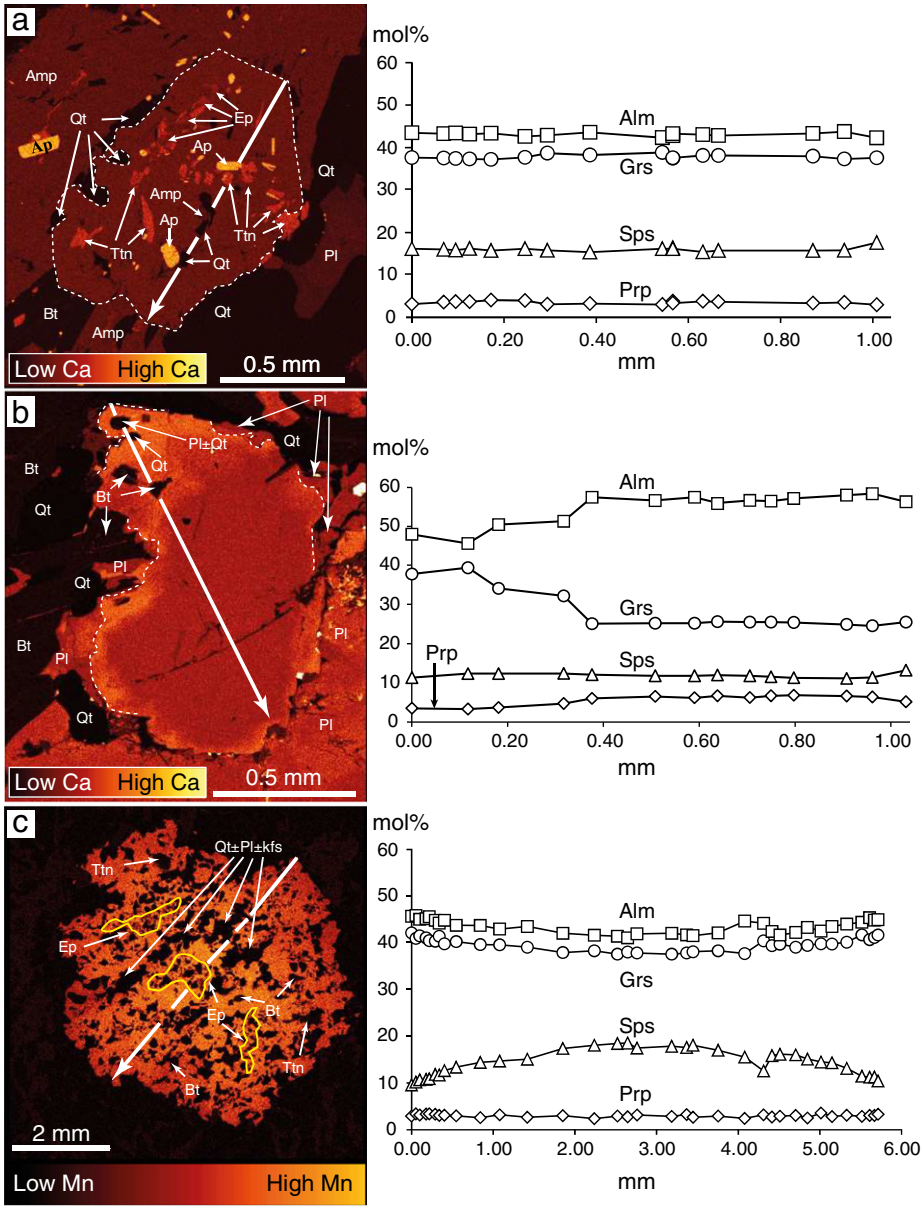

Fig. 7. Garnet chemical maps and profiles. (a) Garnet from Bt + Amp + Grt granitoids (same crystal shown in Fig. 5f); (b) garnet from Bt + Grt granitoids (same crystal shown in Fig. 5d); (c) garnet in MME (same in crystal shown in Fig. 5h); white dashed lines in (a) and (b) show garnet boundaries; for each map thick white arrows indicate the sense of the section analysed; the relative rim to rim zonation patterns are given in the diagram in the left. The maps also indicate the inclusions. More traverses are available at Table OSM1 and Fig. 1 in OSM 2.

these two minerals (Fig. 6h and f). Sericite, formed as a partial replacement after some plagioclase crystals, and very minor replacement after minerals by chlorite, are the only secondary minerals recognized in the rocks.

3.3. Mineral chemistry

All garnets represent almandine–grossular–spessartine solid solutions with ubiquitously low pyrope content (<7 mol%). Grossular (X_{Grs}) and spessartine (X_{Sps}) contents are relatively high, ranging from 24.1 to 43.4 (with 85% > 35 mol%) and from 9.4 to 18.8 mol%, respectively (Table 1 and Table OSM1). The significance of this is discussed in Section 4.2. In more detail, garnets belonging to the Bt + Grt assemblage have compositions within the range $Alm_{41.7–58.5}Grs_{24.1–40.1}Sps_{9.4–18.8}Prp_{1.9–6.9}$. Within the Bt + Amp + Grt granitoids and MMEs, the crystals display a more restricted range of compositions, that is $Alm_{40.1–43.5}Grs_{37.3–43.4}Sps_{13.8–17.2}Prp_{2.7–3.7}$ and $Alm_{40.9–45.7}Grs_{37.4–42.0}Sps_{9.6–18.5}Prp_{2.4–3.6}$, respectively. The great majority (ca. 95%) of the analysed garnets despite having different textures are unzoned (Fig. 7a and 1a in OSM 2). In a few cases where garnets have been found having grossular reverse bell-shape-like profiles (Figs. 7b and 1b in OSM 2), the

Table 1
Summary of the grossular, pyrope, almandine and spessartine content in mol% of magmatic garnets in metaluminous to slightly peraluminous natural granitoids and experimental melts.

Garnet	Grossular	Pyrope	Almandine	Spessartine
Galiléia granitoids[a]	24.1–43.4	1.9–6.9	40.1–58.5	9.4–18.8
Bushy Point Granitoids[b]	33–46	2–6	41–52	10–11
Experimental garnets[c]	20.4–31.5	13.5–35.2	40.7–58.5	0.7–6.8
Worldwide natural garnets[d]	11.8–28.4	1.5–43.8	37.1–72.7	1.4–19.5

[a] This study.
[b] Zen and Hammarstrom (1984a).
[c] Alonso-Perez et al. (2009); Green (1992); Schmidt (1993); Schmidt and Thompson (1996).
[d] Bach et al. (2012); Barnes and Allen (2006); Day et al. (1992); Dawes and Evans (1991); Harangi et al. (2001); Owen and Marr (1990); Samadi et al. (2014).

grossular content increases from core to rim from ca. 25 mol% up to almost 40 mol%. Pyrope and spessartine patterns appear broadly flat. Other zonation is seen in garnet hosted in the MMEs where, a decrease in X_{Sps} from core to rim, from 17.42 to 9.57 mol% is associated by an increase in X_{Grs} and X_{Alm} (from 37.68 to 41.55 mol% and from 41.76 to 44.76 mol%, respectively) (Fig. 7c). It is important to note that the X_{Prp} in all the garnets is constantly low, and Mg# always <0.10. These observations are in agreement with Nalini (1997) who performed the firsts and only mineral chemistry analyses of garnets from the Galiléia.

Analyses of epidotes from the matrix of the granitoids and MMEs show pistacite contents [Ps = $(Fe^{3+}/Fe^{3+} + Al) * 100$] in the range of 14.6–22.7 mol% and 13.9–17.8 mol%, respectively (Fig. 8a and Table OSM3). The Ps content of epidote inclusions within garnets, biotite, plagioclase and amphibole from the granites (9.3–22.2 mol%) and from the MMEs (11.6–17.3 mol%) is slightly wider but overall similar to that of the epidote in the relevant rock matrix. Rare zoisite inclusions in garnet have FeO_{Total} below 2 wt.% and Ps = 3.8–4.2 mol%.

Biotite in Bt + Grt granitoids (Fig. 8b and Table OSM4) exhibits higher Fe# [Fe/(Fe + Mg); 0.63–0.70] than biotite in other assemblages and MMEs, which display Fe# ~ 0.58–0.62. The TiO_2 contents of biotites do not show any significant difference between the different granitoid assemblages and the MMEs, ranging from 1.47 to 3.04 wt.%. The composition of biotite inclusions in garnets is similar to that of biotite in the matrix. Biotite inclusions in garnets from the MMEs have a very narrow range of Fe# and higher titanium contents (1.90–3.00 wt.%) with respect to those in the MMEs matrix (1.10–2.03 wt.%).

Primary white mica crystals have Si contents (3.14–3.22 a.p.f.u.) similar to some low-Si phengites in metamorphosed granitoids (Fig. 8c and Table OSM4) (Evans and Patrik, 1987), although Al_{Tot} (2.62–2.53 a.p.f.u.) and Mg + Fe_{Tot} (0.26–0.37 a.p.f.u.) differ slightly (Fig. 8d). These crystals are also similar in composition to primary muscovite from peraluminous granitoids (Huang et al., 2015; Liu et al., 2014; Miller et al., 1981), but are compositionally distinct from sericitic

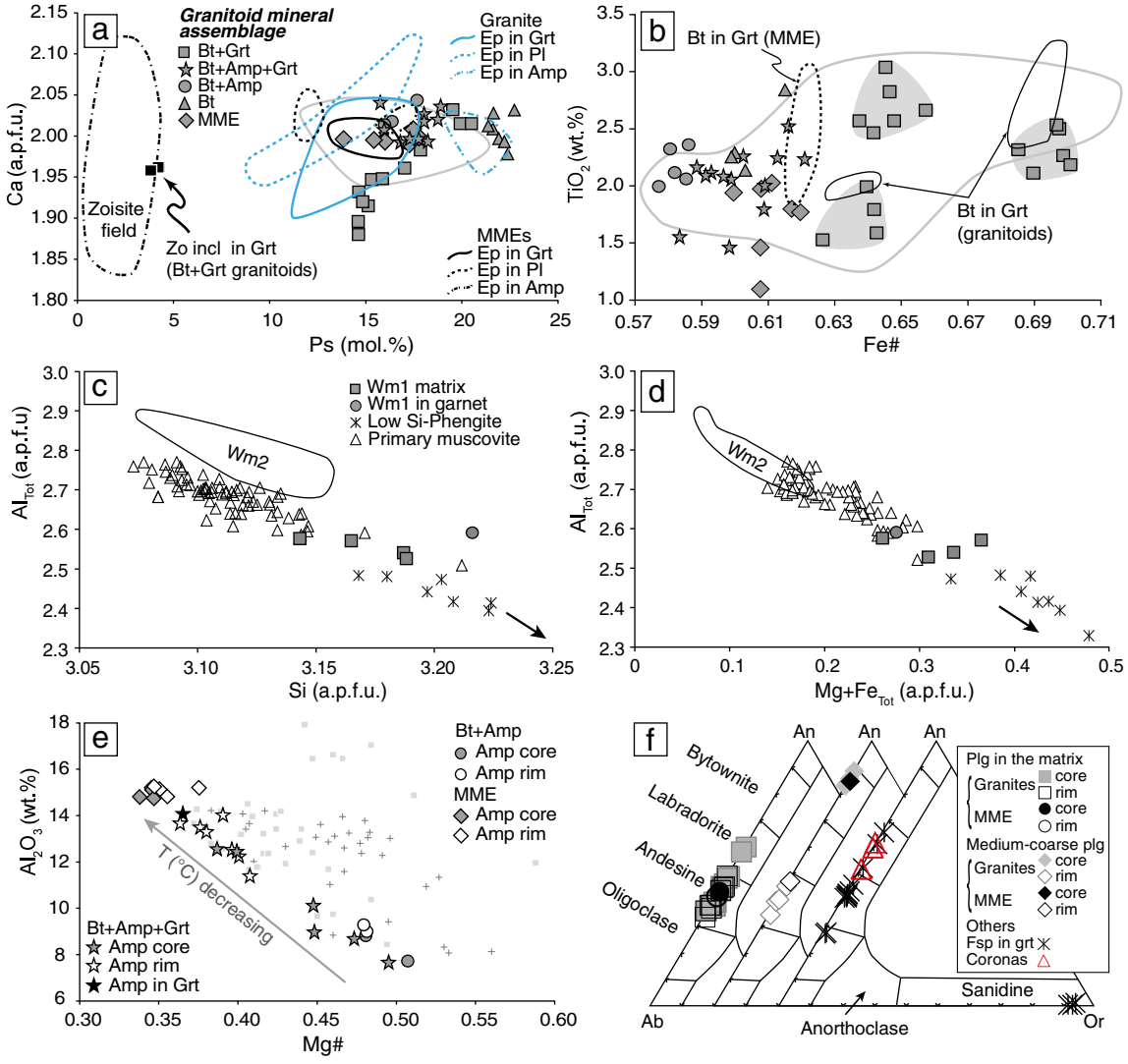

Fig. 8. Mineral chemistry. (a) Epidote composition plotted in a Ca (a.p.f.u.) against their pistacite content [Ps = $(Fe^{3+}/Fe^{3+} + Al) * 100$]; black squares in the grey field are compositions from the inclusion shown in Fig. 6f; zoisite field from high pressure experiments (up to 3.2 GPa) from Patiño-Douce (2005) and Skjerlie and Patiño-Douce (2002); (b) Fe# [Fe/(Fe + Mg)] vs. TiO_2 (wt.%) for biotites; in (a) and (b) thick grey line indicates epidote and biotite analyses performed by Nalini (1997), respectively; (c) and (d) primary and secondary white micas composition are plotted in Si (a.p.f.u.) and Mg + Fe_{Tot} (a.p.f.u.) against Al_{Tot}; other primary muscovites are from peraluminous granitoids (Huang et al., 2015; Liu et al., 2014; Miller et al., 1981) while metamorphic low-Si phengites are from Evans and Patrik (1987); black arrows indicate that some analyses from the latter authors plot below Al_{Tot} = 2.3 (a.p.f.u.) and above Si = 3.25 and Mg + Fe_{Tot} 0.5 (a.p.f.u.); (e) amphibole composition plotted in the Mg# against A_2O_3 (wt.%); grey squares and grey crosses are analyses from Nalini (1997) on amphiboles from Galiléia granitoids and MMEs, respectively; grey arrow indicates the decreasing of temperature as the Mg# decreases (i.e. Alonso-Perez et al., 2009); (f) Ternary An-Ab-Or feldspar classification diagram (after Deer et al., 1992).

products (low Si and higher Al_{Tot}) within plagioclase crystals from granitoids and MMEs.

Using Locock's (2014) amphibole spread sheet classification after the IMA 2012 report of Hawthorne et al. (2012) (Table OSM5), amphiboles are classified as follows: amphiboles from Bt + Amp-granitoids are unzoned and compositionally similar to the ferro-hornblende cores of the amphiboles from Bt + Amp-Grt-granitoids, which instead have rims classified as ferro-pargasite, as is the case for the core of the rare amphibole inclusion in garnet (Fig. 8e). There is a marked variation in Mg# and Al_2O_3 content between the cores and the respective rims of amphiboles from the Bt + Amp + Grt assemblage (Fig. 8e). Mg# in the cores varies between 0.50 and 0.39, while Mg# from the rims have a lower and more restricted range of values (0.36–0.41). As described by Alonso-Perez et al. (2009), this decrease in Mg# is related to decreasing temperature during magma crystallization. In contrast, Al_2O_3 is depleted in the cores (7.68–12.58 wt.%) compared with the respective rims (11.41–14.02 wt.%). The composition of amphibole cores and rims is identical in the MMEs, with a lower Mg# and Al_2O_3 content than amphibole in the granites. Note that the mineralogy of these rocks renders them unsuitable for the application of the Al in hornblende geobarometer, e.g. Hammarstrom and Zen (1986) and Mutch et al. (2016).

Euhedral and subhedral plagioclase crystals together with plagioclase coronas over garnet and inclusions in garnets share the same normal zonation, with labradorite cores and andesine rims (An_{60} to An_{36}; Fig. 8f and Table OSM6). The texturally distinct cores from 10 to 15 mm sized plagioclase found in the Galiléia granites as well as in mafic enclaves have very high An contents (from An_{83} to An_{89}), differing completely from their rims (An_{35} to An_{47}).

3.4. Whole rock geochemistry

Whole rock compositions from Galiléia igneous rocks and mafic enclaves have been previously analysed by Gonçalves et al. (2014), Nalini (1997) and Nalini et al. (2005). Our major and trace element data agree (Table OSM7) with those reported by these authors (Fig. 9). The granitoids here studied are granodiorites with only one tonalite (Fig. 9a). K_2O content (1.76–3.8 wt.%) shows a positive correlation with SiO_2 (62.21–72.04 wt.%) (Fig. 9b) and as expected for I-type granites (e.g. Clemens et al., 2011; Farina et al., 2012), A/CNK (0.97–1.07) and CaO (2.82–6.09 wt.%) are negatively and positively correlated with FeO_{Tot} + MgO (2.96–8.29 wt.%) (Fig. 9c and d, respectively). A negative correlation is also seen with respect to MnO (0.04–0.17 wt.%) (Fig. 9e). Overall, major and trace element composition of the Galiléia granitoids,

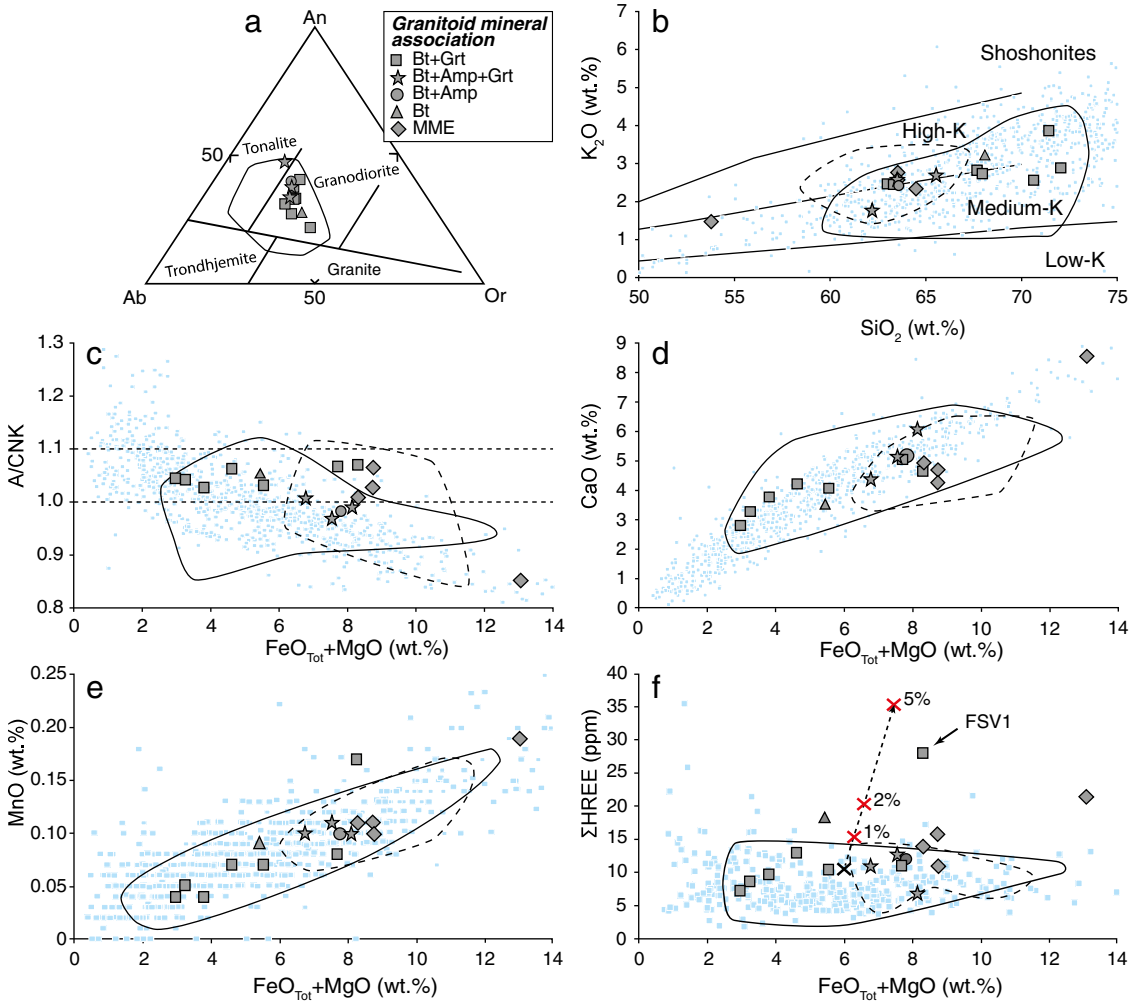

Fig. 9. Whole rock geochemistry. (a) Normative An-Ab-Or diagram (after Barker, 1979) for the Galiléia granitoids; (b) SiO_2 against K_2O; (c), (d), (e) and (f) FeO_{Tot} + MgO is plotted against A/CNK [molar Al/(2Ca + Na + K)], CaO, MnO and ∑HREE, respectively. Plain lines and dotted lines represent compositional fields for granitoids and mafic enclave analyses from Gonçalves et al. (2014) and Nalini (1997), respectively. Light blue squares are metaluminous cordilleran-type I-type granitoids from North and South Patagonian Batholith (Castro et al., 2011; Hervé et al., 2007; Pankhurst et al., 1999), Western and Eastern Peninsular Ranges (Lee et al., 2007), Sierra Nevada Batholith (Bateman et al., 1984; Cecil et al., 2011; Dodge et al., 1982) and Lachlan Fold Belt (Clemens et al., 2011); (e), black dotted arrow indicates the incremental trend in maficity and ∑HREE of a typical cordilleran-type granitoids similar to one of the Galiléia granitoids at which has been added from 1 to 5 vol.% of garnet. Except for one sample (FSV1), the ∑HREE content for the Galiléia granitoids is similar to the cordilleran-type granitoids; see text for further explanation.

match well with those of Cordilleran-type granites worldwide (Fig. 9). Garnet-bearing enclaves have Mg# values ranging between 0.36 and 0.40, whereas the only garnet-free enclave which was analysed and classified as a gabbro displays the highest Mg# (0.46), FeO_{Tot} + MgO (13.07 wt.%) and ∑HREE (10.07 ppm).

4. Discussion

The widespread occurrence of garnet and epidote is the most striking and petrologically interesting characteristic of the Galiléia Batholith. To our knowledge, only one previous study reports magmatic garnet compositions matching those described in this study, that is the Bushy Point granites in south eastern Alaska (Zen and Hammarstrom, 1984a) (Table 1).

4.1. Magmatic garnet, epidote and white mica in the Galiléia batholith

Several lines of field, petrographic and chemical evidence indicate that the garnet crystals in the Galiléia granitoids are magmatic. Firstly, garnet crystals occur in weakly deformed granitoids showing no evidence of metamorphism. Garnet abundance does not correlate with the degree of deformation in the granite and garnet crystals occur as inclusions in large euhedral alkali-feldspar crystals in granites showing porphyritic textures (Fig. 4a). Secondly, garnet abundance does not increase in the proximity of the contact with the Rio Doce metasediments and garnet crystals in the batholith have different compositions from garnet in the metapelites, the former being higher in CaO (Fig. 10). Further simple chemical arguments confirm that garnets in the Galiléia granitoids are neither entrained from the country rocks nor inherited from the source. In fact, the inclusion of 1 to 5 vol.% of source rock garnet in a typical cordilleran-type granite would discernibly increase both the FeO_{Tot} + MgO and ∑HREE of the rock as illustrated in Fig. 9e; this behaviour is not observed for the garnet-bearing samples of the Galiléia batholith. Moreover, the abundance of garnet does not correlate with the SiO_2 and CaO content of the granitoids and their presence is reported from the least (SiO_2 = 58.8 wt.%), to the most evolved (SiO_2 = 72.2 wt.%) garnet-bearing Galiléia granitoid. Furthermore, the garnet-bearing Galiléia granitoids are geochemically identical to many other garnet-free Cordilleran-type granites worldwide.

Finally, the minerals hosted as inclusions within the garnet crystals are the same, both in terms of assemblage and composition, as those constituting the matrix of the granitoids. It is also worth noting that garnet occurrence and/or abundance are not related to the abundance of MMEs in the outcrop, suggesting that garnet did not form in the enclaves as also confirmed by the disequilibrium features acquired by garnet crystals hosted in the enclaves.

Collectively, this evidence demonstrates that garnet in the studied rocks is magmatic. Therefore, we conclude that the presence/absence of this garnet depends on variables other than the rock composition.

In the Galiléia batholith there are two other coexisting minor phases that appear to be magmatic and may be important in understanding the conditions of magma crystallization: epidote and white mica. In agreement with textural observations on magmatic epidotes reported by Schmidt and Poli (2004), Schmidt and Thompson (1996) and Zen and Hammarstrom (1984b), the presence of epidote crystals rimming allanite cores, and their common occurrence in the interstitial sites between the rock forming minerals (amphibole, plagioclase and biotite) point towards a magmatic origin for epidote (e.g. Nalini, 1997). Furthermore, the Ps content of matrix epidote crystals (14.6–22.7 mol%) is very similar to epidote inclusions hosted within rock-forming phases (Ps = 9.3–22.2 mol%), supporting a magmatic origin for both textural varieties of epidote. Based on textural observation we exclude that epidotes (Ps = 9.3–17.4 mol%) included in plagioclase (Fig. 6c) are derived from the alteration of this mineral. In fact, epidote inclusions are ragged, cracked, and commonly zoned showing corroded and/or resorbed rims. Following Chang and Andronicos (2009) and Dawes and Evans (1991), we interpret these inclusions as early magmatic crystals followed by resorption before plagioclase overgrowth during successive magmatic stages. Epidote crystals within the MMEs share similar textural and compositional (Ps = 11.8–17.3 mol%) features with those in the granites, thus they are also interpreted as being magmatic. Finally, despite the fact that the occurrence of white mica overgrowing magmatic biotite and plagioclase could suggest a secondary origin, the presence of white mica as inclusion in the garnet points towards a magmatic origin. Its primary origin is also supported by its chemical composition which is similar to other low-Si phengites and primary muscovites from the literature, but quite different from sericitic products (i.e. late secondary white mica) (Fig. 8c, d).

4.2. Pressure–temperature conditions

4.2.1. Pressure of crystallization

Crystallization experiments and studies on natural metaluminous igneous rocks have shown that garnet with CaO contents above 4 wt.% (and in general with Grs > 10 mol%) records crystallization at pressures above approximately >0.8 GPa (Alonso-Perez et al., 2009; Bach et al., 2012; Barnes and Allen, 2006; Dawes and Evans, 1991; Day et al., 1992; Green, 1972, 1977, 1992; Green and Ringwood, 1968, Green, 1972; Harangi et al., 2001; Samadi et al., 2014 and others). Schmidt and Thompson (1996) investigated garnet stability within a granodiorite and established that the garnet-in reaction is located at a pressure as high as 1.3 GPa and around 800 °C. Garnet stability within granitoid magmas varies as a function of composition as well as pressure and temperature (see also Vielzeuf and Schmidt, 2001). Although no crystallization experiments have produced garnet with grossular contents as high as those observed in the Galiléia garnets (Table 1), similarities between experimental and natural rock studies are in good agreement in indicating that the presence of grossular-rich magmatic garnet within the Galiléia granitoids can be regarded as evidence of crystallization at a pressure above at least 0.8 GPa.

This conclusion is also supported by the occurrence of phengitic white mica and epidote in the Galiléia granitoids. According to Schmidt and Poli (2004) and Schmidt and Thompson (1996), the appearance of epidote in the crystallization sequence of a cooling magma is pressure dependent. These authors demonstrated that epidote is stable above 0.6 GPa, and that its temperature of first crystallization in a cooling magma increases with increasing pressure. In the Galiléia granitoids, epidote is found as a common inclusion in biotite and plagioclase, as a rare inclusion in garnet, and in the matrix between amphibole, plagioclase and biotite. Based on the experiments of

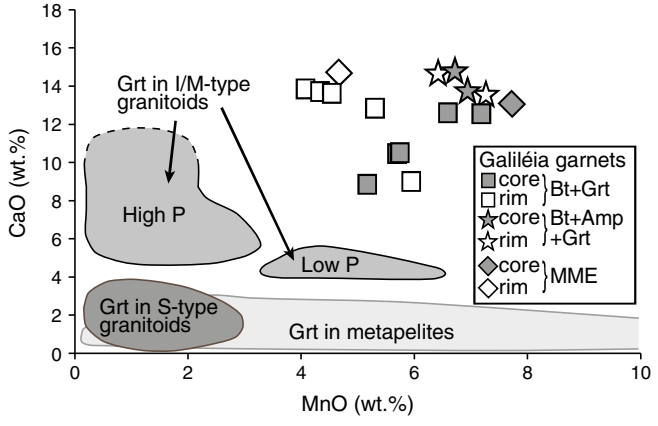

Fig. 10. CaO against MnO wt.% (after Harangi et al., 2001 and Samadi et al., 2014). Note that the upper limit of the area representing the CaO rich-garnets has not been defined, yet. Here and in Fig. 11 only the more representative (core and rim) analyses for the Galiléia garnets are reported.

Schmidt and Thompson (1996), this textural information is consistent with pressure conditions in the range of 0.8–1.0 GPa. Thus the experiments of Alonso-Perez et al. (2009), Green (1992), and Schmidt and Thompson (1996), constrain the stability of garnet + epidote within the Galiléia granitoids to pressures between ca. 0.8 and 1.0 GPa, corresponding to depths of approximately 25–30 km in the lower crust.

4.2.2. The geochemical diversity of the Galiléia garnets

The most striking characteristic of the Galiléia magmatic garnets is their extremely high grossular and spessartine contents reaching 45 mol% and 20 mol%, respectively and constantly low pyrope content (<7 mol%). (Figs. 10 and 11). We compared the chemistry of these crystals with: 1) garnet from crystallization experiments at high pressure (>0.8 GPa) using metaluminous to weakly peraluminous starting materials that were similar in composition to the Galiléia granitoids (Alonso-Perez et al., 2009; Green, 1992; Schmidt, 1993; Schmidt and Thompson, 1996) (Fig. 12), and 2) magmatic garnet from natural metaluminous to weakly peraluminous felsic igneous rocks (Bach et al., 2012; Barnes and Allen, 2006; Dawes and Evans, 1991; Day et al., 1992; Harangi et al., 2001; Owen and Marr, 1990; Samadi et al., 2014; Zen and Hammarstrom, 1984a). We observe that the Galiléia garnets are more grossular-rich and pyrope-poor ($Grs_{24.1–43.4}Prp_{1.9–6.9}Alm_{40.1–58.5}Sps_{9.4–18.8}$) than both experimental ($Gro_{20.4–31.5}Prp_{13.5–35.2}Alm_{40.7–58.5}Sps_{0.7–6.8}$) and natural crystals ($Gro_{11.8–28.4}Prp_{1.5–43.8}$ $Alm_{37.1–72.7}$ $Sps_{1.4–19.5}$) (Table 1). However, the Galiléia garnets are compositionally identical to the magmatic garnet crystals ($Grs_{33–46}Prp_{6–6}Alm_{41–52}Sps_{10–11}$) from the metaluminous

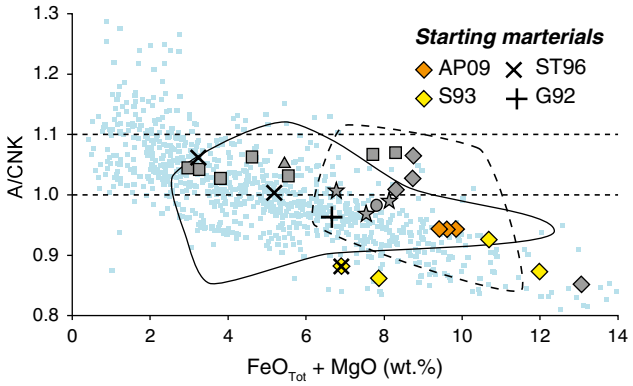

Fig. 12. A/CNK vs FeO_{Tot} + MgO diagram. Comparison between Galiléia granitoids, Cordilleran-type granites and staring materials used in high pressure crystallization experiments. AP09: Alonso-Perez et al. (2009); G92: Green (1992); S93: Schmidt (1993); ST96: Schmidt and Thompson (1996). Other symbols are as in Fig. 9.

Bushy Point Granitoids (A/CNK 0.91–1.10; SiO_2 59.6–72.6 wt.%; CaO 1.3–6.2 wt.%) (Zen and Hammarstrom, 1984a). From Fig. 11a and b, it appears that only the garnet which crystallized in experiments at a temperature of 650 °C and at high water contents (≥10 wt.%) has compositions close to those of some of the Galiléia garnets.

In the experimental garnet, the pyrope content decreases at decreasing temperatures while the almandine contents show the opposite

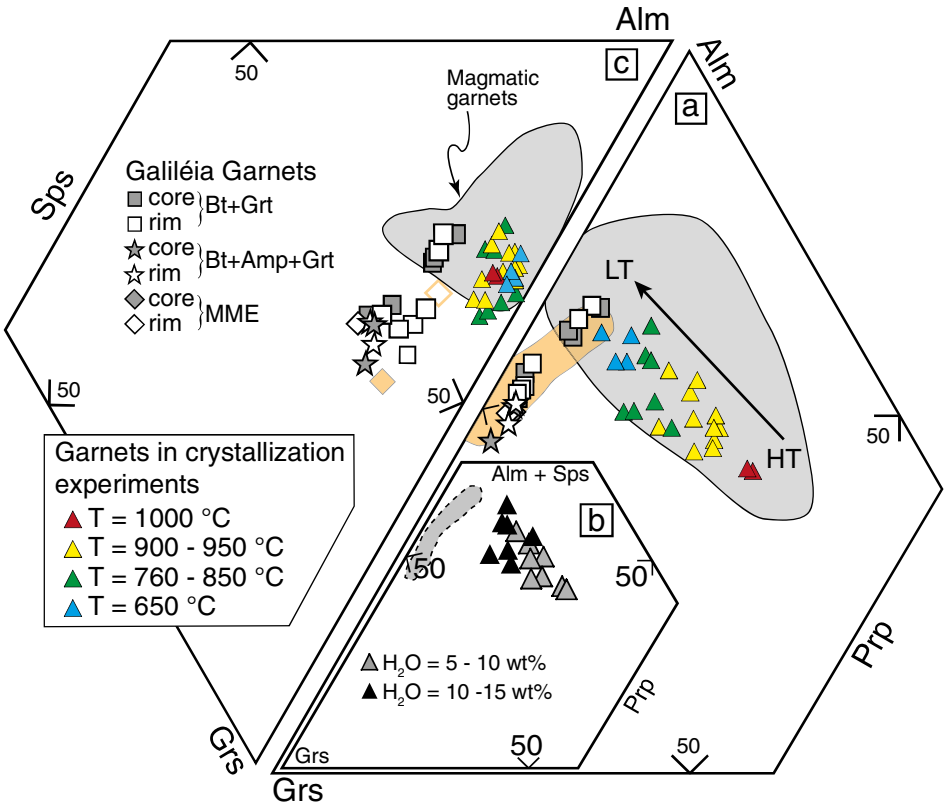

Fig. 11. Comparison between Galiléia, experimental and natural magmatic garnets. (a) Almandine-grossular-pyrope classification diagrams. Experimental garnets (coloured triangles) are those in equilibrium with the metaluminous and slightly peraluminous experimental melts. These garnets are reported according to their crystallization temperature. Grey field: magmatic garnets in volcanic as well as granitic metaluminous to weakly peraluminous rocks (Bach et al., 2012; Barnes and Allen, 2006; Dawes and Evans, 1991; Day et al., 1992; Harangi et al., 2001; Owen and Marr, 1990; Samadi et al., 2014). Light orange field: Bushy Point garnets from Bushy Point Granitoids, Alaska (Zen and Hammarstrom, 1984a). Note that for these garnets the grossular field was redrawn from Fig. 70 of Zen and Hammarstrom (1984a). Grey arrow indicates the trend from high (HT) to low (LT) temperature garnets. (b) Alm + Sps–Grs–Prp diagram. The same experimental garnets used in (a), here are plotted considering the water content of the experimental melt. Grey dotted area represents the part of the diagram covered by the Galiléia granitoids. Note that for the garnets of Green (1992) and those at 650 °C of Schmidt (1993) there is no data relative to the water of the melt. (c) Almandine–grossular–spessartine diagram. Symbols as in a). Note that only for one Bushy point garnet the spessartine content has been reported (filled and empty light orange diamonds are core and rim, respectively).

behaviour, being negatively correlated with temperature (Fig. 11a, b and c). These relationships might account for the low pyrope content exhibited by the Galiléia garnet, but data retrieved from experimental studies do not explain the origin of the high spessartine and especially high grossular content observed in the garnet of the Galiléia batholith. The only experiments that seem to suggest a negative correlation between the grossular content and temperature are those performed by Alonso-Perez et al. (2009) at 1.2 GPa. These authors observed an increase of grossular content from 20.7 to 31.5 mol% as a consequence of a decrease in temperature from 1000 to 850 °C and to an increase of the water content of the melt from 5.4 to 11.0 wt.%. Nevertheless, any clear correlation is observed considering the spessartine content.

A possible explanation for the high grossular content of the Galiléia garnet might come from Schmidt and Thompson (1996). They observed that in metaluminous granitic systems, quartz and epidote start crystallizing at temperature around 655 and 700 °C, respectively, with epidote stable in water saturated melts (≥10 wt.%). Thus the high grossular content of garnet crystals together with their epidote and quartz inclusions, might suggest that these garnets were produced by a process of dissolution and recrystallization in which garnet was continuously reacting and re-equilibrating with a melt that was evolving towards low temperature (<650–700 °C) and high water contents (>10 wt.%). The same explanation could also apply for the spessartine content, which increases as the magma evolves (Miller and Stoddard, 1981).

4.3. Geotectonic implications: a new tectonic model for the Araçauí Orogen?

It is worth remarking that garnet is widespread in the Galiléia batholith characterizing outcrops that are in many cases more than 10 km apart. This simple observation indicates that similar high-pressure conditions were attained in the whole batholith.

Since little is known about the P–T–t history of the host Rio Doce metasediments, any attempts to understand its relationships with the Galiléia granitoids remain quite speculative. Nevertheless, some observations can be made.

So far it has been highlighted that the Galiléia granitoids record high pressure (>0.8 GPa) crystallization and emplacement in the lower crust. This implies that since 630 Ma the crust underneath this portion of the Araçuaí Orogen was already at least 25–30 km thick and relatively cool. This is in contrast with the hot thermal regime registered from the neighbour Carlos Chagas Batholith, located 50 km to the east, within the eastern domain (Fig. 1b; Melo et al., 2017). In fact, this batholith records granulite-facies metamorphism (0.9–1.0 GPa and 790–820 °C) at 570 Ma, age at which: 1) the Galiléia granitoids were already crystallized (632–570 Ma; Tedeschi et al., 2016) and 2) the Araçuaí Orogen was experiencing syn-collisional tectonics (Pedrosa-Soaeres et al., 2011). Overall, this would imply that the Galiléia high pressure granitoids should also record granulite-facies metamorphism. Instead, these rocks are weakly deformed and do not show any evidence of metamorphic overprinting. This has two possible and different tectonic implications: either the Galiléia granitoids at 570 Ma were already exhumed at shallower crustal levels, which prevented them from undergoing granulite facies metamorphism, or alternatively these garnet-bearing granitoids and the Carlos Chagas batholith belonged to different lithospheric domains joined together after 570 Ma. The last hypothesis is supported by the presence of a poorly-studied major thrust separating the central and eastern domains (see black bold dotted line in Fig. 1b; e.g. Vauchez et al., 2007).

Eventually, the same field, petrographic and chemical features so far reported for the garnet-bearing Galiléia granitoids have been also described for the garnet-bearing Bushy point granites (Zen and Hammarstrom, 1984a). Noteworthy these granitoids are located presumably within the accretionary prism and/or fore-arc settings of the north-coastal British Columbia subduction zone, south eastern Alaska. In such settings, high pressure, low temperature (Brown, 2006) and water-rich magmas are readily achievable. Notably, some of these conditions are those suggested by this work. It is then possible that both the garnet-bearing Galiléia and Bush Point granitoids represent "rare" garnet- and epidote-bearing metaluminous Cordilleran-I-type granites which can only form in a fore-arc setting.

5. Conclusions, remarks and open questions

The presence of magmatic garnet crystals together with the presence of magmatic epidotes indicates a high-pressure crystallization environment probably between 0.8 and 1.0 GPa, corresponding to depths of approximately 25–30 km. These findings would also imply that at 630 Ma the crust below the Araçuaí orogen was already overthickened and cool. High grossular and spessartine content in garnet together with its epidote and quartz inclusions might be due to reaction between the crystal and the evolving granitic magma towards low temperature and high water content. Some resorption textures also indicate that these minerals were consumed before complete crystallization. Eventually, what has been highlighted throughout this work has opened new challenging questions like: 1) why no experiments so far were able to reproduce the composition of the Galiléia garnets? 2) How much water was present in the melt from which the grossular- and spessartine-rich Galiléia garnets crystallized? 3) How much melt (vol.%) was still present during garnet crystallization at high-pressure and temperature of ca. 650–700 °C? And eventually, despite there is a clear connection between the garnet-bearing Galiléia granitoids and the fore-arc related garnet-bearing Bushy Point and, 4) what is the most reliable geodynamic scenario for having within the same orogenic system, at the same pressure condition and at the same geological time, two contrasting thermal regimes? More studies must be done in order to answer to all of the above questions.

Supplementary data to this article can be found online at http://dx.doi.org/10.1016/j.lithos.2017.02.017.

Acknowledgements

The authors wish to acknowledge funding from CNPq (401334/2012-0, 302058/2015-0, 402852/2012-5) and FAPEMIG (APQ03943, RPQ-0067-10-RDP 00063-10) grants and Edital UFOP Auxilio a pesquisador 2015. FN thanks Conselho Nacional de Desenvolvimento Científico e Tecnológico for the financial support (CNPq 164000/2013-5). G. Stevens gratefully acknowledges National Research Founding support through the SARChI programme. Careful and constructive reviews from Ramin Samadi and Patrizia Fiannacca have stimulated and strongly improved the quality of the manuscript. We also thank Editor Nelson Eby for the editorial handling. C. Albert, C. Aguilar, C. Martinez, G. Gonçalves and M. Melo are kindly acknowledged for their technical and moral support. L. Ziberna and M. Casanova are also thanked for their scientific and friendly support. This work is part of the first author's doctorate project.

References

Alkmim, F.F., Marshak, S., Pedrosa-Soares, A.C., Peres, G.G., Cruz, S.P.C., Whittington, A., 2006. Kinematic evolution of the Araçuaí-West Congo orogen in Brazil and Africa: nutcracker tectonics during the Neoproterozoic assembly of Gondwana. Precambrian Research 149, 43–64.

Allan, B.D., Clarke, D.B., 1981. Occurrence and origin of garnets in the South Mountain Batholith, Nova Scotia. The Canadian Mineralogist 19, 19–24.

Alonso-Perez, R., Müntener, O., Ulmer, P., 2009. Igneous garnet and amphibole fractionation in the roots of island arcs: experimental constraints on andesitic liquids. Contributions to Mineralogy and Petrology 157, 541–558.

Arth, J.G., Barker, F., Stern, T.W., 1988. Coast Batholith and Taku Plutons near Ketchikan, Alaska: petrography, geochronology, geochemistry, and isotopic character. American Journal of Science 288-A, 461–489.

Bach, P., Smith, I.E.M., Malpas, J.G., 2012. The origin of garnets in andesitic rocks from the Northland Arc, New Zealand, and their implication for sub-arc processes. Journal of Petrology 53, 1169–1195.

Barker, F., 1979. Trondjemites: definition, environment and hypotheses of origin. In: Barker, F. (Ed.), Trondhjemites, Dacites and Related Rocks. Elsevier, Amsterdam, pp. 1–12.

Barnes, C.G., Allen, C.M., 2006. In: Snoke, A.W., Barens, C.G. (Eds.), Depth of Origin of Late Middle Jurassic Garnet Andesite, Southern Klamath Mountains, California. Geological Studies in the Klamath Mountains Province, Califronia and Oregon: A volume in honour of William P. Irwin Geological Society of American Special Papers 410, pp. 269–286.

Barnes, C.G., Frost, C.D., Nordgulen, Ø, Prestvik, T., 2012. Magma hybridization in the lower crust: possible consequences for deep-crustal magma mixing. Geosphere 8, 518–533.

Bateman, P.C., Dodge, F.C.W., Bruggman, P.E., 1984. Major oxide analyses, CIPW norms, modes, and bulk specific gravities of plutonic rocks from the Mariposa 1 x 2 degrees sheet, central Sierra Nevada, California. United State Geological Survey OF 84-0162 (59 pp.).

Brandon, A.D., Creaser, R.A., Chacko, T., 1996. Constraints on rates of granitic magma transport from epidote dissolution kinetics. Science 271, 1845–1848.

Brown, M., 2006. Duality of thermal regimes is the distinctive characteristics of plate tectonics since the Neoarchean. Geology 34, 961–964.

Castro, A., Moreno-Ventas, I., Fernández, C., Vujovich, G., Gallastegui, G., Heredia, N., Martino, R.D., Becchio, R., Corretegé, L.G., Díaz-Alvarado, J., Garcías-Arias, M., Liu, D.-Y., 2011. Petrology and SHRIMP U-Pb zircon geochronology of Cordilleran granitoids of the Bariloche area, Argentina. Journal of South American Earth Sciences 32, 508–530.

Cecil, M.R., Rotberg, G.L., Ducea, M.N., Saleeby, J.B., Gehrels, G.E., 2011. Magmatic growth and batholithic root development in the northern Sierra Nevada, California. Geosphere 8, 592–606.

Chang, J.M., Andronicos, C.L., 2009. Constraints on the depth of generation and emplacement of a magmatic epidote-bearing quartz diorite pluton in the Coast Plutonic Complex, British Columbia. Terra Nova 21, 480–488.

Clarke, B.D., 2007. Assimilation of xenocrysts in granitic magmas: principles, processes, proxies, and problems. The Canadian Mineralogist 45, 5–30.

Clemens, J.D., Stevens, G., Farina, F., 2011. The enigmatic sources of I-type granites: the peritectic connexion. Lithos 126, 174–181.

Cunningham, W.D., Marshak, S., Alkmim, F.F., 1996. Structural style of basin inversion at mid-crustal levels: two transects in the internal zone of the Brasiliano Araçuaí Belt, Minas Gerais, Brazil. Precambrian Research 77, 1–15.

Dalquist, J.A., Galindo, C., Pankhurst, R.J., Rapela, C.W., Alasino, P.H., Saavedra, J., Fanning, C.M., 2007. Magmatic evolution of the Peñón Rosado granite: petrogenesis of garnett-bearing granitoids. Lithos 95, 177–207.

Dawes, R.L., Evans, B.W., 1991. Mineralogy and geothermobarometry of magmatic epidote-bearing dyke, Front Range, Colorado. Geological Society of America Bulletin 103, 1017–1031.

Day, R.A., Green, T.H., Smith, I.E.M., 1992. The origin and significance of garnet phenocryst and garnet-bearing xenoliths in Miocene calc-alkaline volcanics from Northland, New Zealand. Journal of Petrology 33, 125–161.

Deer, W.A., Howie, R.A., Zussman, J., 1992. An Introduction to the Rock-forming Minerals. 2nd eds. Longman, Harlow.

Dodge, F.C.W., Millard Jr., H.T., Helsheimer, H.N., 1982. Compositional variations and abundances of selected elements in granitoid rocks and constituent minerals, Central Sierra Nevada, Batholith, California. Geological Survey Professional Paper. 1248, p. 29.

Erdmann, S., Jamieson, R.A., Macdonald, M.A., 2009. Evaluating the origin of garnet, cordierite and biotite in granitic rocks: a case study from the South Mountain Batholith, Nova Scotia. Journal of Petrology 50, 1477–1503.

Evans, B.W., Patrik, B.E., 1987. Phengite-3T in high pressure metamorphosed granitic orthogneisses, Seaward Peninsula, Alaska. The Canadian Mineralogist 25, 141–158.

Evans, B.W., Vance, J.A., 1987. Epidote phenocrysts in dacitic dikes, Boulder Country, Colorado. Contributions to Mineralogy and Petrology 96, 178–185.

Farina, F., Stevens, G., Dini, A., Rocchi, S., 2012. Peritectic phase entrainment and magma mixing in the late Miocene Elba Island laccolith-pluton-dyke complex (Italy). Lithos 153, 243–260.

Gonçalves, L., Farina, F., Lana, C., Pedrosa-Soares, A.C., Alkmim, F.F., Nalini Jr., H.A., 2014. New U-Pb ages and lithochemical attibutes of the Ediacaran Rio Doce magmatic arc, Araçuaí confined orogen, southeastern Brazil. Journal of South American Earth Sciences 52, 1–20.

Green, T.H., 1972. Crystallization of calc-alkaline andesite under controlled high-pressure hydrous condition. Contributions to Mineralogy and Petrology 34, 150–166.

Green, T.H., 1977. Garnet in silicic liquids and its possible use as a P-T indicator. Contributions to Mineralogy and Petrology 65, 59–67.

Green, T.H., 1992. Experimental phase equilibrium studies of garnet-bearing I-type volcanics and high-level intrusives from Northland, New Zealand. Transactions of the Royal Society of Edinburgh: Earth Sciences 83, 429–438.

Green, T.H., Ringwood, A.E., 1968. Origin of garnet phenocryst in calc-alkaline rocks. Contributions to Mineralogy and Petrology 18, 163–174.

Hammarstrom, J.M., Zen, E-na, 1986. Aluminum in hornblende: an empirical igneous geobarometer. American Mineralogist 71, 1297–1313.

Harangi, S.Z., Downes, H., Kosa, L., Szabo, C.S., Thirlwall, M.F., Mason, P.R.D., Mattey, D.P., 2001. Almandine garnet in calc-alkaline volcanic rocks of the Northern Pannonian basin (Eastern-Central Europe): geochemistry, petrogenesis and geodynamic implications. Journal of Petrology 42, 1813–1843.

Harrison, T.N., 1988. Magmatic garnets in the Cairngorm granite, Scotland. Mineralogical Magazine 52, 659–667.

Hawthorne, F.C., Oberti, R., Harlow, G.E., Maresh, W.V., Martin, R.F., Schumacher, J.C., Welch, M.D., 2012. IMA report, nomenclature of the amphibole supergroup. American Mineralogist 91, 2031–2048.

Hervé, F., Pankurst, R.J., Fanning, C.M., Calderón, M., Yaxely, G.M., 2007. The south Patagonian batholith: 150 my of granite magmatism on a plate margin. Lithos 97, 373–394.

Holdaway, M.J., 1972. Thermal stability of Al-Fe epidote as a function of fO_2 and Fe content. Contributions to Mineralogy and Petrology 37, 307–340.

Huang, H.-Q., Li, X.-H., Li, Z.-X., Li, W.-X., 2015. Formation of Jurassic South China Large Granitic Province: insights from the genesis of the Jiufeng pluton. Chemical Geology 401, 43–58.

Lackey, J.S., Romero, G.A., Bouvier, A.-S., Valley, J.W., 2012. Dynamic growth of garnet in granitic magmas. Geology 40, 171–174.

Lee, C.T.A., Morton, D.M., Kistler, R.W., Barid, A.K., 2007. Petrology and tectonics of Phanerozoic continent formation: from island arc to accretion and continental arc magmatism. Earth and Planetary Science Letters 263, 370–387.

Liou, J.G., 1973. Synthesis and stability relations of epidote, $Ca_2Al_2FeSi_3O_{12}(OH)$. Journal of Petrology 14, 381–413.

Liu, Z.-C., Wu, F.-Y., Ji, W.-Q., Wang, J.-G., Liu, C.-Z., 2014. Petrogenesis of the Ramba leucogranite in the Tethyan Himalaya and constraints on the channel flow model. Lithos 208-209, 118–136.

Locock, A.J., 2014. An Excel spreadsheet to classify chemical analyses of amphiboles following the IMA 2012 recommendations. Computers and Geosciences 62, 1–11.

Melo, M.G., Stevens, G., Lana, C., Pedrosa-Soares, A.C., Frei, D., Alkmim, F.F., Alkmin, L.A., 2017. Two cryptic anatectic events within a syn-collisional granitoid from the Araçuaí orogen (southeastern Brazil): Evidence from the polymetamorphic Carlos Chagas batholith. Lithos 277, 51–71.

Miller, C.F., Stoddard, E.F., 1981. The role of manganese in the paragenesis of magmatic garnet: an example from the Old Woman-Piute Range, California. The Journal of Geology 89, 233–246.

Miller, C.F., Stoddard, E.F., Bradfish, L.J., Dollase, W.A., 1981. Composition of plutonic muscovite: genetic implications. The Canadian Mineralogist 19, 25–34.

Mondou, M., Egydio-Silva, M., Vauchez, A., Raposo, M.I.B., Bruguier, O., Oliveira, A.F., 2012. Complex, 3D strain patterns in a synkinematic tonalite batholith from the Araçuaí Neoproterozoic orogen (Eastern Brazil): evidence from combined magnetic and isotopic chronology studies. Journal of Structural Geology 39, 158–179.

Mutch, E.J.F., Blundy, J.D., Tattitch, B.C., Cooper, F.J., Brooker, R.A., 2016. An experimentally study of amphibole stability in low-pressure granitic magmas and a revised Al-in-hornblende geobarometer. Contributions to Mineralogy and Petrology 171, 85.

Nalini Jr., H.A., 1997. Caractérisation de suítes magmatiques néoprotzoïques de la région de Conselheiro Pena et Galiléia (Minas Gerais, Brésil). Etude géochimique et structurale des suítes Galiléia et Urucum et relation avec les pegmatites á élémentes rares associées. Ecole National Supérieure de Mines de Paris et de Saint Etienne, St Etienne, p. 237 (PhD thesis).

Nalini Jr., H.A., Bilal, E., Paquette, J.-L., Pin, C., Machado, R., 2000. Géochronologie U-Pb et géochimie isotopique Sr-Nd des granitoïdes néoprotérozoïques des Suites Galiléia et Urucum, vallée du Rio Doce, Sud Est du Brésil. Computes Rendus 331, 459–466.

Nalini Jr., H.A., Machado, R., Bilal, E., 2005. Geoquímica e petrogênese da suíte Galiléia: exemplo de magmatismo tipo-I metaluminoso pre-colisional Neoproterózoico da região do médio do Vale de Rio Doce (MG). Revista Brasileira de Geociencias 35, 23–34.

Nalini Jr., H.A., Machado, R., Endo, I., Bilal, E., 2008. A importância da tectônica transcorrente no alojamento de granitos pré a sincolisional na região do vale do médio Rio Doce: o exemplo da suítes graníticas Galiléia e Urucum. Revista Brasileira de Geociencias 38, 741–752.

Owen, J.V., Marr, R.A., 1990. Contrasting garnet parageneses in a composite Grenvillian granitoid pluton, Newfoundland. Mineralogical Magazine 54, 367–380.

Pankhurst, R.J., Weaver, S.D., Hervé, F., Larrondo, P., 1999. Mesozoic–Cenozoic evolution of the North Patagonian Batholith in Aysén, southern Chile. Journal of the Geological Society of London 156, 673–694.

Paterson, S.R., Fowler Jr., K.T., Schmidt, K.L., Yoshinobu, A.S., Yuan, E.S., Miller, R.B., 1998. Interpreting magmatic fabric in plutons. Lithos 44, 53–82.

Patiño-Douce, A.E., 2005. Vapour absent melting of tonalite at 15–32 kbar. Journal of Petrology 46, 275–296.

Pedrosa-Soares, A.C., De Campos, C.P., Noce, C., Silva, L.C., Novo, T., Roncato, J., Medeiros, S., Castañeda, C., Queiroga, G., Dantas, E., Dussin, I., Alkmim, F.F., 2011. Late Neoproterozoic-Cambrian granitic magmatism in the Araçuaí Orogen (Brazil), the Eastern Brazilian Pegmatite Province and related mineral resources. Geological Society of London Special Publication 350, 25–51.

Pedrosa-Soares, A.C., Noce, C.M., Wiedemann-Leonardos, C.M., Pinto, C.P., 2001. The Araçuaí-West Congo Orogen in Brazil: an overview of a confined Orogen formed during Gondwanaland assembly. Precambrian Research 110, 307–323.

Pedrosa-Soares, A.C., Wiedemann-Leonardos, C.M., 2000. Evolution of the Araçuaí belt and its connection to the Ribeira Belt, Eastern Brazil. In: Cordani, U.G., Milani, E.J., Tomaz, Filho A., Campos, D.A. (Eds.), Tectonic Evolution of South America, International Geological Congress, Rio de Janeiro, pp. 265–285.

Petitgirard, S., Vauchez, A., Egydio-Silva, M., Bruguier, O., Camps, P., Monié, P., Babinski, M., Mondou, M., 2009. Conflicting structural and geochronological data from the Ibituruna quartz-syenite (SE Brazil): effect of protracted orogeny and slow cooling rate? In: Chardon, D., Ray, P. (Eds.), Hot Orogens Special Issue Tectonophysics 477, pp. 174–196

Richter, F., Lana, C., Stevens, G., Buick, I., Pedrosa-Soares, A.C., Alkmim, F.F., Cutts, K., 2015. Sedimentation, metamorphism and granite generation in a back-arc region: record from the Ediacaran Nova Venécia Complex (Araçuaí Orogen, Southeastern Brazil). Precambrian Research 272, 78–100.

Samadi, R., Mirnejad, H., Kawabata, H., Harris, C., Valizadeh, M.V., Gazel, E., 2014. Magmatic garnet in the Triassic (215 Ma) Dehnow pluton of NE Iran and its petrogenetic significance. International Geology Review 56, 596–621.

Schmidt, M.W., 1993. Phase relations and compositions in the tonalite as a functions of pressure: an experimental study at 650°C. American Journal of Science 293, 1011–1060.

Schmidt, M.W., Poli, S., 2004. Magmatic epidote. Reviews in Mineralogy and Geochemistry 56, 399–430.

Schmidt, M.W., Thompson, A.B., 1996. Epidote in calc-alkaline magmas: an experimental study of stability, phase relationships, and the role of epidote in magmatic evolution. American Mineralogist 81, 462–474.
Skjerlie, K.P., Patiño-Douce, A.E., 2002. The fluid-absent partial melting of zoisite-bearing quartz eclogite from 1.0 to 3.2 GPa; implications for the melting in thickened continental crust and for subduction-zone processes. Journal of Petrology 43, 291–314.
Tedeschi, M., Novo, T., Pedrosa-Soares, A., Dussin, I., Tassinari, C., Silva, L.C., Gonçalves, L., Alkmim, F., Lana, C., Figueiredo, C., Dantas, E., Medeiros, S., De Campos, C., Corrales, F., Heilbron, M., 2016. The Ediacaran Rio Doce magmatic arc revisited (Araçuaí-Ribeira orogenic system, SE Brazil). Journal of South American Earth Sciences 68, 167–186.
Vauchez, A., Egydio-Silva, E., Babinski, M., Tommasi, A., Uhlein, A., Liu, D., 2007. Deformation of a pervasively molten middle crust: insights from the Neoproterozoic Ribeira-Araçuaí orogen (SE Brazil). Terra Nova 19, 278–286.
Vernon, R.H., 2007. Problems in identifying restite in S-type granites in southeastern Australia, with speculation on source of magma and encalves. The Canadian Mineralogist 45, 147–178.
Vieira, V.S., 2007. Significado do grupo do Rio Doce no context do Orógeno Araçuaí. (PhD Thesis). Universidade Federal de Minas Gerais, Belo Horizonte, p. 117.
Vielzeuf, D., Schmidt, M.W., 2001. Melting relations in hydrous systems revisited: application to metapelites, metagreywakes and metabasalts. Contributions to Mineralogy and Petrology 141, 251–267.
Villaros, A., Stevens, G., Buick, I.S., 2009. Tracking S-type granite from source to emplacement: clues from garnet in Cape Granite suite. Lithos 112, 217–235.
Whitney, D.L., Evans, B.W., 2010. Abbreviations for names of rock-forming minerals. American Mineralogist 95, 185–187.
Xu, L., Xiao, Y., Wu, F., Li, S., Simon, K., Wörner, G., 2013. Anatomy of garnets in a Jurassic granite from the south-eastern margin of the North China Craton: magma sources and tectonic implication. Journal of Asian Earth Science 78, 198–221.
Zen, E-an, Hammarstrom, J.M., 1984a. Mineralogy and petrogenetic model for the tonalite pluton at Bushy Point, Revillagigedo Island, Ketchikan 1° × 2° quadrangle, southeastern Alaska. United State Geological Survey 939, 118–123.
Zen, E-an, Hammarstrom, J.M., 1984b. Magmatic epidote and its petrologic significance. Geology 12, 515–518.